iScience

Article

The network response to Egf is tissue-specific

Graphical abstract

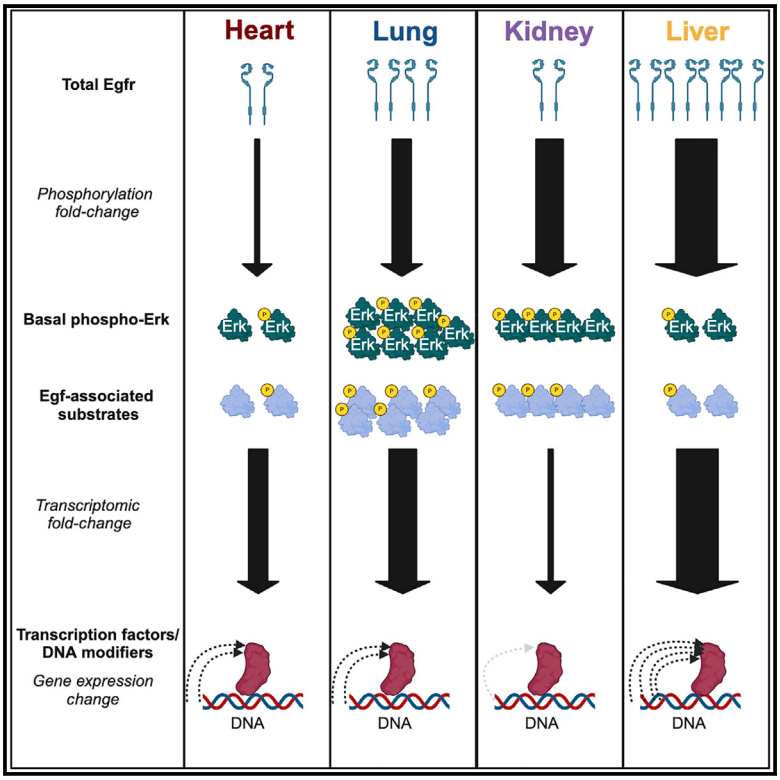

Highlights

- Egf-induced signaling is tissue-specific at the proteomic and transcriptomic levels
- Tissues have distinct baseline Egf-associated signaling profiles
- Baseline levels of Egf signaling do not correlate with induced changes in signaling
- Linear mixed modeling can be applied to identify tissue-specific signaling

Authors

Beatrice W. Awasthi, João A. Paulo, Deborah L. Burkhart, ..., J. Wade Harper, Steven P. Gygi, Kevin M. Haigis

Correspondence

kevin_haigis@dfci.harvard.edu

In brief

Molecular biology; Bioengineering; Systems biology

Awasthi et al., 2025, iScience *28*, 112146
April 18, 2025
https://doi.org/10.1016/j.isci.2025.112146

CellPress

iScience

CellPress
OPEN ACCESS

Article

The network response to Egf is tissue-specific

Beatrice W. Awasthi,[1,2] João A. Paulo,[3] Deborah L. Burkhart,[4] Ian R. Smith,[3,8] Ryan L. Collins,[4,6,7] J. Wade Harper,[3] Steven P. Gygi,[3] and Kevin M. Haigis[4,5,9,*]

[1]Center for Systems Biology, Department of Radiation Oncology, and Center for Cancer Research, Harvard Medical School and Massachusetts General Hospital, Boston, MA 02114, USA
[2]Broad Institute of MIT and Harvard, Cambridge, MA 02142, USA
[3]Department of Cell Biology, Harvard Medical School, Boston, MA 02115, USA
[4]Department of Cancer Biology, Dana Farber Cancer Institute, Boston, MA 02215, USA
[5]Department of Medicine, Harvard Medical School, Boston, MA 02215, USA
[6]Department of Medical Oncology, Dana-Farber Cancer Institute, Boston, MA 02115, USA
[7]Cancer Program, Broad Institute of M.I.T. and Harvard, Cambridge, MA 02115, USA
[8]Present address: Velia Therapeutics, San Diego, CA, USA
[9]Lead contact
*Correspondence: kevin_haigis@dfci.harvard.edu
https://doi.org/10.1016/j.isci.2025.112146

SUMMARY

Epidermal growth factor receptor (Egfr)-driven signaling regulates fundamental homeostatic processes. Dysregulated signaling via Egfr is implicated in numerous disease pathologies and distinct Egfr-associated disease etiologies are known to be tissue-specific. The molecular basis of this tissue-specificity remains poorly understood. Most studies of Egfr signaling to date have been performed *in vitro* or in tissue-specific mouse models of disease, which has limited insight into Egfr signaling patterns in healthy tissues. Here, we carried out integrated phosphoproteomic, proteomic, and transcriptomic analyses of signaling changes across various mouse tissues in response to short-term stimulation with the Egfr ligand Egf. We show how both baseline and Egf-stimulated signaling dynamics differ between tissues. Moreover, we propose how baseline phosphorylation and total protein levels may be associated with clinically relevant tissue-specific Egfr-associated phenotypes. Altogether, our analyses illustrate tissue-specific effects of Egf stimulation and highlight potential links between underlying tissue biology and Egfr signaling output.

INTRODUCTION

Signaling driven by the epidermal growth factor receptor (Egfr) plays a key role in growth, development, and tissue repair in response to injury.[1–5] At the same time, chronic pathological activation of Egfr or its downstream effector pathways is implicated in several disease pathologies, including cancer, tissue fibrosis, and heart failure.[6–9] Anecdotally, Egfr-driven pathologies appear to be highly tissue-specific.[6,8,10–12] The underlying reasons for differences between tissues are poorly understood.

Due to the far-reaching and diverse consequences of dysregulated Egfr signaling, gaining insight into the nuances of Egfr signaling and its outcomes within specific tissue contexts is of interest. A major limitation for understanding the tissue-specific nature of Egfr signaling has been the lack of consistent *in vivo* models that could be used to compare Egfr-driven signaling between distinct living tissue settings. Although many *in vitro* studies have provided insight into Egfr-associated substrates, Egfr-regulated gene expression, signaling kinetics, and disease associations, these studies are limited in their ability to facilitate conclusions about Egfr signaling in living tissues.[13–16] Furthermore, while several mouse models have been deployed to study Egfr signaling, inconsistencies between the models used in different studies have made it difficult to determine the extent to which tissue biology influences the outcome of Egfr-associated signaling.[7,17–19] Further characterization of Egfr signaling in specific tissue contexts could help improve the therapeutic options for more precisely treating Egfr-associated pathologies in a tissue-specific manner.

Homeostatic tissue-specific expression patterns have been documented in the context of the phosphoproteome and proteome,[20] transcriptome,[21] and epigenome.[22] We hypothesized that such differences in underlying tissue biology could be associated with tissue-specific Egfr-driven signaling patterns. Here, our objective was to better understand the association between tissue biology and ligand-stimulated Egfr-driven signaling. To that end, we carried out a comparison of short-term responses to Egfr stimulation between tissues using the Egfr ligand Egf. Egf is a growth factor that signals exclusively via Egfr and plays a central role in growth, development, and wound healing.[2,3,23,24] The specificity of Egf for Egfr renders it ideal to compare tissue responses to controlled Egfr activation in a temporally and environmentally controlled setting. We compared the output of Egf-driven signaling between the heart, lung, kidney, and liver in adult mice. These tissues were selected because they exhibit a range of known Egfr-associated functions and disease associations, as well as varied Egf-stimulated proliferative capabilities. Of these

tissues, the liver is known to be the most regenerative—with Egf playing a major role in driving the regeneration—whereas the heart is the least regenerative.[25,26] The lung has a notably higher frequency of somatic mutations in the *EGFR* gene in cancers than do the other tissues.[11] Also, among these four tissues, the lung has the highest frequency of oncogenic mutations in one of the major effector pathways of Egfr, the MapkMapk pathway.

Our goal was to identify and compare signaling networks stimulated by Egf within each tissue and to characterize their association with intrinsic tissue biology. To that end, phosphoproteomic and proteomic analysis with tandem mass tag (TMT) labeling was used in conjunction with transcriptomic analysis to build tissue-specific landscapes of Egf-driven signaling responses in each tissue. Furthermore, since both *EGFR* and MAPK pathway mutations are more frequently found in lung cancers than in cancers of the other tissues, we hypothesized that Egf-driven Mapk signaling may have certain tissue-specific properties within the lung that make the lung more susceptible to these mutations. Therefore, we additionally combined Egf stimulation with Mapk inhibition to evaluate Egf-driven Mapk signaling between the four tissues. Subsequently, we investigated how native tissue biology was associated with the Egf-stimulated phosphoproteome in each tissue. While spatial phosphoproteomic changes in response to Egf stimulation within murine kidney and liver samples have been previously reported,[27] this report is, to our knowledge, the first multi-omics comparison of Egf-driven changes between tissues. Altogether, our results shed light on tissue-specific patterns in Egf-driven signaling and offer insight into potential therapeutically relevant links between intrinsic tissue biology and general Egfr signaling.

RESULTS

Proteome-wide, relative quantification of Egf-stimulated phosphorylation changes within single-tissue plexes

Our first objective was to establish a global phosphorylation landscape of short-term Egf signaling within the heart, lung, kidney, and liver. We treated 10-week-old female mice with Egf by retro-orbital injection and rapidly harvested the tissues for phosphoproteomic and proteomic analysis 15 min following injection (Figure 1A). For all phosphoproteomic and proteomic experiments, we made use of TMT labeling. Labeling of samples with the isobaric TMT reagents enables the multiplexing of samples within a single mass spectrometry run. Phosphopeptide and peptide levels between all samples in a single TMT plex can be directly compared. Here, all Egf-stimulated and control samples for a single tissue were included within a single TMT plex. Phosphopeptide quantification was performed using in-house software, as reported previously[28] (see STAR Methods). Fold-changes in phosphorylation of peptides within Egf-stimulated samples were calculated relative to the vehicle control samples within each tissue; these fold-changes were then compared across tissues.

Overall, 10,833 singly phosphorylated peptides were detected in the lung, 9,504 in the kidney, 7,302 in the liver, and 6,888 in the heart (Figure 1B, top; Table S1). There were also 1,973 multi-phosphorylated peptides detected in our dataset (not shown), but, due to the ambiguity in the localization of these sites, we restricted our subsequent analysis to singly phosphorylated peptides. We first analyzed the spectrum of phosphopeptides and proteins detected in our tissues. Although there was diversity in specific phosphopeptides detected within each tissue (Figure 1C, left panel), most proteins corresponding to the phosphopeptides were detected in all tissues (Figure 1C, middle panel; Tables S1 and S2). Additionally, we analyzed changes in Egfr phosphorylation to verify its activation within all four tissues. Egfr activation results in the autophosphorylation of numerous tyrosine residues and positive feedback phosphorylation at Egfr (Ser993). Induction of Ser993 phosphorylation within each tissue relative to baseline was detected in all four tissues, along with autophosphorylation of several tyrosine residues within individual tissues, indicating successful stimulation of Egfr in all tissues (Figure 1D).

To ensure inter-replicate consistency of phosphorylation changes within each tissue, phosphopeptides with a high coefficient of variation (CV) across replicates were filtered out (see STAR Methods; Figures S1A and S1B). Following filtering, all samples clustered together by tissue using both hierarchical clustering and principal-component analysis (PCA) of the phosphorylation fold-changes for the Egf-treated versus vehicle control samples for each tissue (Figures 1E and 1F). Notably, the replicate number appeared to drive the variation along principal component 2, indicating that biological variability within different mice was preserved, even across different TMT plexes.

The magnitude of Egf-induced phosphorylation is tissue-specific

For most of the phosphopeptides that were detected in more than one tissue, the fold-change in phosphorylation was positively correlated across tissues, as indicated by the values for the correlation coefficient (r) (Figure 2A). Nevertheless, the magnitudes of the fold-changes were notably different between particular pairs of tissues. For example, when comparing the heart and the kidney, more than half of the phosphopeptides either increase or decrease in both tissues, however, the fold-changes in the heart are generally lower than in the kidney.

We next identified statistically meaningful Egf-induced fold-changes in phosphopeptide levels within each tissue using MSstatsPTM,[29] which identifies significant phosphorylation changes between samples using linear mixed models. These models incorporate variation from biological replicates, technical replicates, and fractions of samples analyzed by mass spectrometry. Changes in phosphopeptide abundance were adjusted for changes in total protein level to ensure that the phosphopeptide fold-changes between samples were not affected by differences in protein abundance. Fold-changes calculated by MSstatsPTM correlated highly with the mean fold-change calculated using in-house software (Figure S2). The linear mixed modeling analysis performed by MSstatsPTM indicated that the liver had the highest number of phosphopeptides with significant phosphorylation changes, with 7.8% of the phosphoproteome increased and 2.7% decreased in response to Egf stimulation. In the kidney and lung, 5.3% and 4.1% were increased and 0.6% and 0.5% were decreased. The heart had the fewest significant phosphorylation changes, with a total of 46 significantly changed

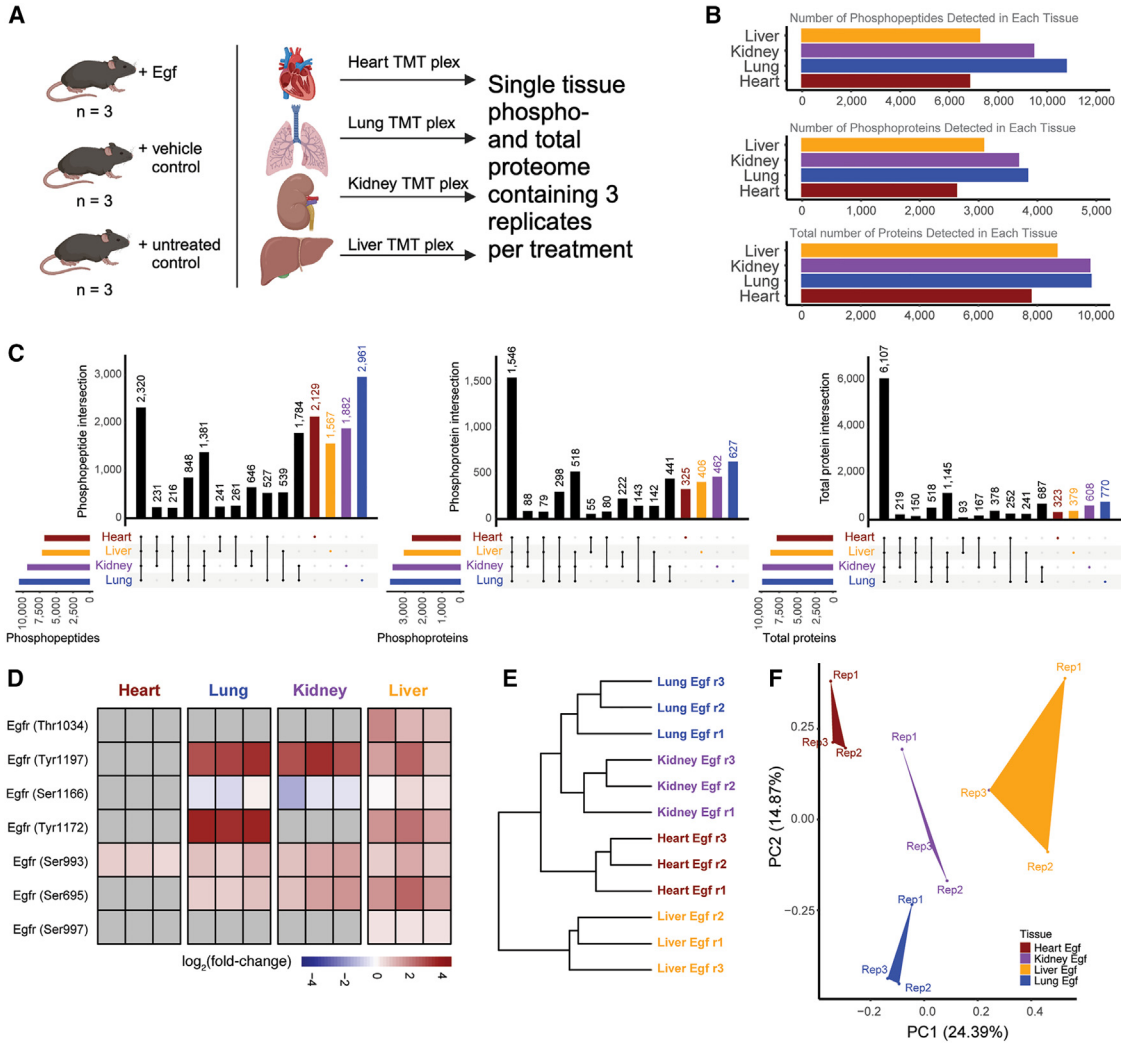

Figure 1. Egf-induced phosphoproteomes vary across tissues

(A) Schematic of treatments and structure of TMT plexes (created with BioRender.com).

(B) Total number of phosphopeptides (top), phosphoproteins (middle), and proteins (bottom) detected in each tissue.

(C) Phosphopeptides (left), phosphoproteins (middle), and proteins (right) detected in each combination of tissues.

(D) Log_2(fold-change) in phosphorylation of various sites on Egfr detected in each tissue. Values shown are the log_2(fold-change) in phosphorylation of each site for each Egf-treated replicate relative to the mean phosphorylation level of the 3 vehicle control replicates in each tissue.

(E) Hierarchical clustering and (F) principal component analysis of fold-changes in response to Egf stimulation for each replicate relative to the mean of the 3 vehicle control replicates.

(0.6% increased and only 1 site significantly decreased in phosphorylation) (Figure 2B; Tables S3–S6).

Out of more than 17,000 phosphopeptides that were detected across the four tissues, only 12 were significantly changed in all four, whereas hundreds were significantly changed in only one tissue or a subset of tissues (Figure 2C; Table S7). For phosphopeptides that were not detected in all tissues, it was impossible to discern whether their absence was due to a lack of phosphorylation in those tissues or simply a lack of detection. Therefore, we performed an additional analysis on the subset of phosphopeptides that was detected in all tissues. Out of the 2,320 phosphopeptides detected in all tissues, most significantly changed phosphopeptides were also significantly changed in only one tissue or a subset (Figure 2C). Combined with the observation that a select number of phosphopeptides were also changed in different directions between tissues (Figure 2A), these observations indicated that, while Egf stimulation commonly induced phosphorylation of many phosphopeptides across tissues, each tissue responded to Egf with a unique quantitative combination of phosphorylation fold-changes.

Egf induces significant phosphorylation of proteins within distinct functional ontologies between tissues

To assess how the quantitative differences in Egf-induced phosphorylation of proteins would influence Egf-induced behaviors across tissues, we next compared the functions of

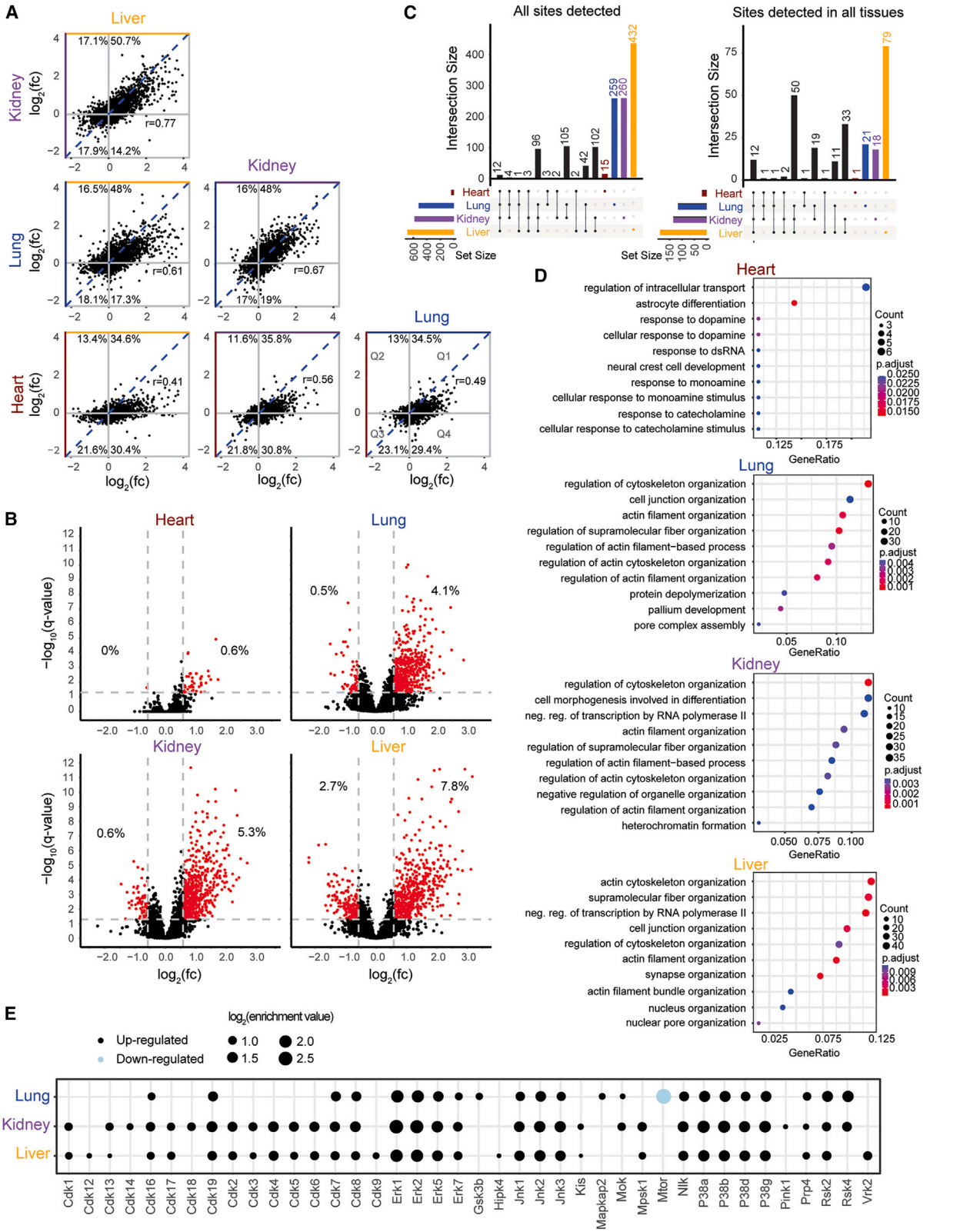

(legend on next page)

proteins with significant phosphorylation changes in response to Egf stimulation between tissues. We performed gene ontology analysis for the biological processes and molecular functions of differentially phosphorylated proteins within each tissue and compared the top enriched ontologies between tissues. All phosphoproteins and proteins detected within each tissue, irrespective of their detection in other tissues, were included in this analysis to ensure the most complete representation of ontologies for each tissue. In the lung, kidney, and liver, the top 10 enriched ontologies for biological process included functions related to structural integrity (Figure 2D). These included "regulation of cytoskeleton organization" and ontologies associated with actin filament organization. "Regulation of intracellular transport" and responses to various stimuli were significantly enriched in the heart (Figure 2D). Notably, in the kidney and liver, "negative regulation of transcription by RNA polymerase II" was within the top 10 enriched biological processes. Additionally, numerous transcription and DNA-binding-associated ontologies were significantly enriched in the molecular function gene ontology analysis of the liver and kidney, including "transcription factor binding" and "RNA polymerase II transcription regulatory region sequence-specific DNA binding" (Figure S3). In contrast, no transcription or DNA-binding-associated molecular functions were significantly enriched among the proteins changed in phosphorylation in response to Egf stimulation in the heart or lung (Figure S3). Rather, only "actin binding" was significantly enriched among these proteins in the heart, and a combination of actin binding and nucleoside-triphosphatase-associated functions were significantly enriched among those in the lung (Figure S3).

Thus, while the direction of Egf-induced fold-changes and enrichment of cytoskeleton-associated proteins among Egf-regulated phosphoproteins were shared across tissues, this gene ontology analysis suggested that the relative extent to which Egf affected the phosphorylation of proteins involved in transcriptional regulation might differ between tissues. Specifically, phosphorylation changes within the transcription and DNA binding-associated phosphoproteome appeared more enriched in the kidney and liver than in the heart and lung. This observation suggested that, at the phosphoproteome level, Egf may prime different tissues for gene expression changes to different extents.

Egf activates core kinase programs across tissues, but the extent of activation is tissue-specific

We also asked how the kinase programs induced by Egf stimulation compared across the tissues in our analysis. To investigate these kinase programs, we performed kinase enrichment analysis on the Egf-induced phosphoproteome within each tissue to assess which kinase programs were likely activated in response to Egf. Kinase enrichment analysis uses $\log_2$(fold-change) of phosphorylation of the entire phosphoproteome as input to predict serine/threonine kinases with likely upregulation or downregulation in activity.[30] In the liver, kidney, and lung, many kinases were predicted to be significantly activated or inactivated. Activation of Mapk kinase family proteins, including Erk family, Jnk family, and p38 family proteins, was universally predicted across the lung, kidney, and liver. Of these, Erk1/2 were the kinases with the greatest predicted increase in activity in all three tissues (Figure 2E). This observation supported the conclusion that stimulation of Mapk signaling is a shared response to Egf binding across epithelial tissues.

At the same time, certain kinases were uniquely predicted to be up- or downregulated within each tissue. In general, the kidney and liver had a higher number of kinases with predicted enriched activity compared with the lung. Notably, several cyclin-dependent kinase (Cdk) proteins, which are involved in cell cycle progression, were predicted to be significantly activated in the liver and kidney, while fewer were predicted to be significantly activated in the lung (Figure 2E). Concurrently, in the lung, activity of mTOR—a downstream target of the PI3K pathway, a known Egfr effector—was predicted to significantly decrease in response to Egf, whereas in the kidney and liver, Egf slightly suppressed predicted mTOR activity, although the change was not significant (Figure 2E; data not shown).[31] Taken together, these predictions supported the notion that Egf triggers Mapk-associated phosphoproteomic changes via the activation of related kinase programs. Furthermore, Egf may simultaneously significantly suppress activity of the parallel PI3K/AKT Egf effector pathway specifically in the lung, but not significantly in the kidney and liver. This analysis also showed a notably

Figure 2. Proportion of significant Egf-induced phosphoproteomic changes is tissue-specific

(A) Log_2(Egf-induced fold-change) of each phosphopeptide detected in pairs of tissues. Phosphorylation fold-changes for each Egf-treated replicate were calculated relative to the mean of all vehicle control replicates, and the Egf-treated fold-changes were then averaged. Average fold-changes are plotted. The blue line is at y = x. Phosphopeptides in quadrants 1 and 3 (quadrants are denoted in the lung versus heart plot on the lower right) were changed in the same direction in response to Egf within pairs of tissues, whereas phosphopeptides in quadrants 2 and 4 were changed in different directions.

(B) Volcano plots showing the $-\log_{10}(q\text{-value})$ versus $\log_2$(fold-change) ($\log_2$(fc)) in phosphorylation of each phosphopeptide detected in each tissue following Egf stimulation relative to vehicle control. Significantly changed sites (q-value <0.05 and abs($\log_2$(fc) > $\log_2$(1.5)) are shown in red. MSstatsPTM was used for significance analysis, and q-values and fold-changes calculated using MSstatsPTM are plotted.

(C) Significantly changed phosphorylation sites detected in each combination of tissues. The left plot shows all sites detected in each TMT plex irrespective of its detection in other plexes, and the right plot shows only sites detected in all 4 TMT plexes.

(D) Gene ontology analysis of biological processes of proteins with significantly changed phosphopeptides following Egf stimulation within each tissue. Significance was determined using MSstatsPTM. The top 10 ontologies for each tissue are shown.

(E) Kinase activity enrichment analysis of the lung, kidney, and liver following Egf-stimulation. For the enrichment analysis, phosphorylation fold-changes for each Egf-treated replicate were calculated relative to the mean of all vehicle control replicates, and the Egf-treated fold-changes were then averaged; the $\log_2$(average) was used as input for the analysis. Kinases with downregulated activity are shown in blue and kinases with upregulated activity in black. Kinases with significantly changed activity (adjusted enrichment p-value of <0.05) are shown.

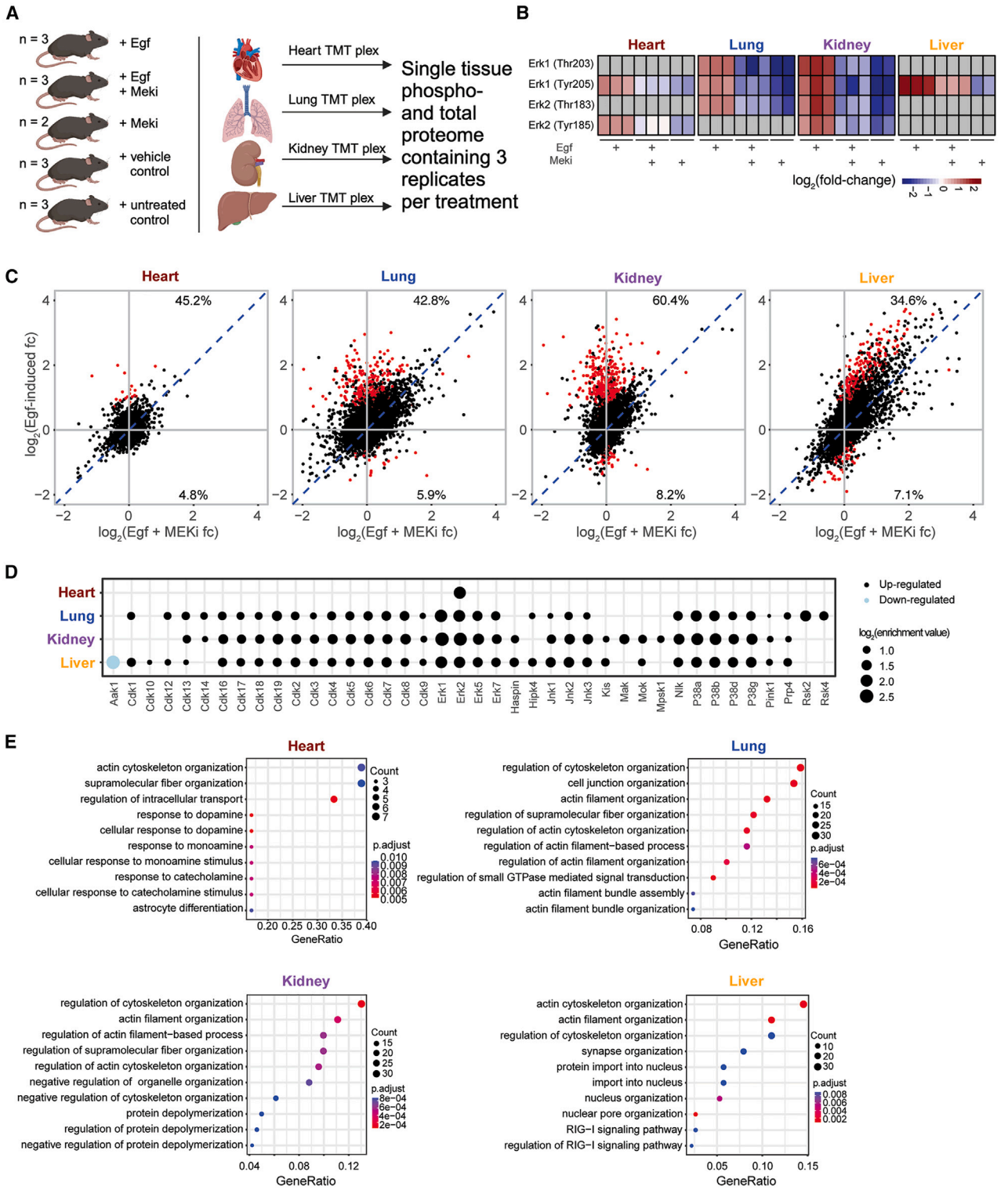

Figure 3. Proportion of significant Mapk-driven Egf-induced phosphorylation changes varies between tissues

(A) Schematic of TMT plexes (created with BioRender.com).

(B) Log_2(fold-change) in phosphorylation of Erk detected in each tissue. Values shown are the log_2-(fold-change) in phosphorylation of each site for each Egf-treated replicate relative to the mean phosphorylation level of the 3 vehicle control replicates in each tissue.

(legend continued on next page)

stronger Egf-induced cell cycle-associated kinase response in the liver and kidney than in the lung.

Mapk involvement in driving Egf-stimulated changes varies between tissues

Given the universality of Mapk activation—but not the other effector pathways—in our tissues, we next asked whether the Mapk pathway induces similar changes across tissues, or whether Egf could induce tissue-specific Mapk-driven effects. To specifically evaluate the contribution of the Mapk pathway to the Egf-stimulated phosphoproteomic response between tissues, we treated mice with Egf in combination with the Mek inhibitor PD-0325901 (Meki) or Meki alone in our single tissue TMT plexes (Figure 3A). In the heart, lung, and kidney, Erk phosphorylation in both the Egf + Meki and Meki alone groups was notably lower than in the vehicle control (Figure 3B). Conversely, in the liver, Erk phosphorylation in the Egf + Meki group was lower than that in the Egf alone group, but higher than vehicle control, indicating that the level of Mek inhibition was insufficient to fully block Egf-stimulated Mapk signaling (Figure 3B). Therefore, our subsequent results for the liver should be interpreted with caution, as the percentage of Erk-dependent sites may have been higher were it not for insufficient Mapk inhibition.

Again, we used MSstatsPTM to identify peptides that were significantly differentially phosphorylated (q-value < 0.05, abs($\log_2$(fold-change)) > $\log_2$(1.5)) between the Egf + Meki and Egf alone groups and found that 50%, 48.7%, 69.2%, and 41.7% of significant Egf-driven phosphorylation changes in the heart, lung, kidney, and liver were Mek-dependent (Figure 3C). Likewise, of phosphopeptides detected in all tissues, the kidney had the highest percentage of significantly Egf-affected phosphopeptides that were significantly Mek-dependent (data not shown here). For a side-by-side comparison of Mapk-dependence among significantly Egf-affected phosphopeptides between tissues, we focused on significantly Egf-affected phosphopeptides detected in both kidney and lung, where there were both a high number of Egf-affected phosphopeptides and effective Mek inhibition. Interestingly, 80% of phosphopeptides significantly affected by Egf in both the lung and kidney were found to be Mek-dependent in the kidney, whereas only 68% of these phosphopeptides were Mek-dependent in the lung (Figure S4). These differences suggested that Mapk signaling may be more crucial in some tissues, such as the kidney, than in others in driving the response to Egf stimulation. Of the phosphopeptides that were detected in all tissues, but uniquely activated in the lung or kidney, 52% and 67% were Mek-dependent within each tissue, suggesting that the Mapk pathway is more likely to regulate core processes affecting all tissues in response to Egf stimulation, rather than tissue-specific Egf-stimulated processes (Figure S4).

Most Egf-stimulated functions and kinase programs are Mapk-dependent in all tissues

To identify Mapk-dependent kinase programs stimulated by Egf in each tissue, we performed kinase enrichment analysis on the fold-differences between Egf-stimulated and Egf + Meki-treated samples. This confirmed significantly lower predicted activity of Mapk family proteins, including the Erk proteins, in all Egf + Meki-treated samples (Figure 3D). Additionally, the activity of Cdk family proteins in all tissues was predicted to be Mapk-dependent, based on significant predicted Cdk activity in Egf-treated samples compared with Egf + Meki-treated samples (Figure 3D). Because pErk levels in the lung, heart, and kidney are even lower than baseline in the Egf + Meki groups, kinases that were not enriched in activation in the Egf versus vehicle comparison were enriched in this analysis. The activity of these kinases was likely partially dependent on Mek, even in the absence of Egf stimulation.

We also performed gene ontology analysis to identify Mapk-dependent biological processes stimulated by Egf in each tissue. To do this, we used as input proteins that were significantly changed in phosphorylation in response to Egf that also had significant fold-differences in phosphorylation level between the Egf-treated and Egf + Meki-treated groups. The ontologies for Mapk-dependent proteins with the highest gene ratios within each tissue included structure-associated groups, including regulation of cytoskeleton organization and actin filament organization (Figure 3E).

Taken together, this experiment suggests that, while the percentage of significantly Egf-affected phosphopeptides that are Mapk-dependent appeared to differ between tissues, the role of the Mapk pathway in mediating Egf-stimulated functions was similar across tissues. Specifically, Mapk signaling was predicted to be primarily involved in organization-related process between tissues. This observation also suggests that the tissue-specificity observed in the ontologies enriched in the tissues stimulated with Egf alone was likely either a result of other pathways or unique combinations of pathway activation between tissues.

(C) Scatterplots of $\log_2$(fold-changes) in phosphopeptide levels following Egf stimulation versus $\log_2$(fold-changes) following Egf + Meki in each tissue. Phosphorylation fold-changes for each treatment group replicate were calculated relative to the mean of vehicle control replicates, and the fold-changes were averaged and plotted. Significantly different phosphopeptides between the two conditions that were also significantly Egf-affected are shown in red. Percentages reflect the percentage of significantly Egf-affected phosphopeptides that were significantly decreased (top) and increased (bottom) following Egf stimulation + Meki.

(D) Kinase enrichment analysis of the phosphorylation fold-changes between Egf-treated and Egf + Meki-treated samples for each tissue. For the enrichment analysis, phosphorylation fold-changes for each Egf and Egf + Meki-treated replicate were calculated relative to the mean of all vehicle control replicates, the average fold-change of each treatment group was calculated, the fold-difference between the average Egf and Egf + Meki-treated groups was calculated, and the $\log_2$(fold-difference) was used as input. Kinases with predicted significantly decreased activity (adjusted enrichment p-value of <0.05) in Egf-treated samples relative to Egf + Meki-treated samples are shown in blue and kinases with predicted significantly upregulated activity are shown in black.

(E) Gene ontology analysis of proteins that have phosphopeptides with significant Egf-induced phosphorylation fold-changes relative to vehicle control and for which the phosphorylation fold-change is significantly different between the Egf-treated and Egf + Meki-treated groups for each tissue. Significant phosphorylation fold-changes were identified using MSstatsPTM.

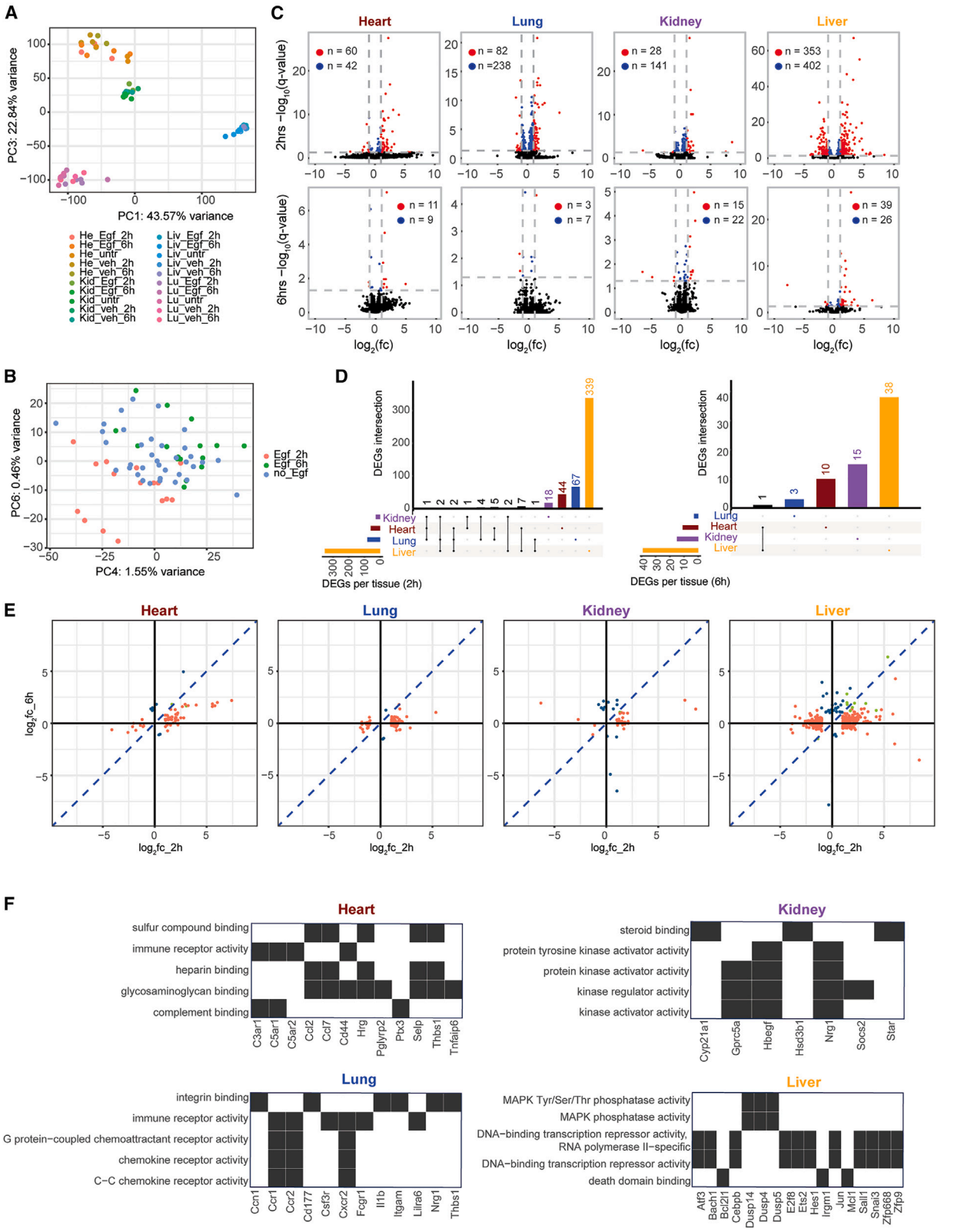

(legend on next page)

Magnitudes of Egf-stimulated transcriptional output are tissue-specific

We next asked whether a similar level of tissue-specificity to the Egf-stimulated phosphoproteome existed at the transcriptomic level. To address this question, we established a landscape of the Egf-stimulated transcriptome for each tissue using RNA sequencing (RNA-seq) (Table S8). We were specifically interested in sustained gene expression changes in response to Egf, as we hypothesized that these would be the ones more likely associated with a phenotypic response. To investigate these changes, we stimulated mice with Egf (n = 4) or vehicle control (n = 3) and collected tissues for RNA-seq at 2 and 6 hours (2 h and 6 h) following injection. Three untreated control mice were also included, resulting in a total of 68 samples with transcriptional profiles from RNA-seq.

We first performed PCA on the entire transcriptomic dataset to evaluate the relationships between the groups in our experiment. To evaluate sources of variation in our dataset, we examined the correlation between each principal component (PC) and tissue type, treatment (e.g., Egf-treated versus no Egf), and treatment at each time point (e.g., Egf, vehicle, or untreated at 2 h or 6 h). As expected, tissue type was the largest source of variation and all samples separated by tissue along the first three PCs (Figure S5; Figure 4A). After accounting for inter-tissue differences, we noted that the next largest source of unexplained transcriptional variance was explained by substantial negative correlation between the "Egf_2 h" and "Egf_6 h" across PC4-6, suggesting that the timing of Egf treatment represents a strong source of variation in gene expression levels (Figure S5). Indeed, the 2 h Egf and 6 h Egf treatment groups noticeably separated on a plot of PC4 against PC6, with 1.55% and 0.46% percent of the variation in the data explained by PC4 and PC6, respectively (Figure 4B). The Egf-treated and no Egf treatment groups appeared to correlate with PC8 most strongly (Figure S5). Thus, overall, this analysis suggested time-point-associated differences between the genes expressed 2 h and 6 h following Egf stimulation across tissues.

Due to the strong transcriptomic differences between tissues noted in the PCA, we normalized gene expression data within each tissue prior to performing differential gene expression analysis in response to Egf stimulation at each time point. Consistent with the phosphoproteomic analysis, the liver had the highest number of transcriptional changes at 2 h following Egf stimulation, with 353 differentially expressed genes (DEGs) at FDR <0.05 and abs($\log_2$(fold-change)) >1 at 2 h following Egf stimulation (Figure 4C; Table S9). The lung and heart had fewer, with 82 and 60 DEGs after 2 h (Figure 4C; Tables S10 and S11). Remarkably, although the kidney had the second-highest number of significant phosphorylation changes following Egf stimulation, it had the fewest significant transcriptomic changes at 2 h following stimulation, with only 28 DEGs (Figure 4C; Table S12). This observation demonstrated the importance of using multi-omics approaches to study ligand-stimulated changes within different tissues, as the type of modification (e.g., phosphoproteomic versus transcriptomic) induced by the ligand may vary between tissues. There was notably little overlap between the significant DEGs at each time point between tissues, which further supported a high level of tissue-specificity in the Egf-induced transcriptional response (Figure 4D). In all tissues, fewer significant DEGs were detected at the 6 h time point at FDR <0.05 and abs($\log_2$(fold-change)) >1 (Figure 4C; Tables S13–S16). Notably, the significant DEGs at 2 h and 6 h following Egf stimulation within each tissue were largely distinct from one another (Figure 4E). This time point variation is consistent with what was seen in the PCA along PC4 and PC6 (Figure 4B). Specifically, the expression of most significant DEGs at 2 h decreased by 6 h, whereas the most significant DEGs at 6 h were not increased at the 2 h mark, supporting nuanced temporal control of Egf-induced gene expression (Figure 4E).

Egf-stimulated transcriptional functions are tissue-specific

To evaluate the functional classifications of the significant DEGs induced within each tissue at each time point, we performed gene ontology analysis. In the liver, significantly upregulated DEGs at 2 h following Egf stimulation were enriched in DNA-binding transcription-associated activities, Mapk phosphatase activity, and death domain binding within the top 5 enriched molecular functions. Genes contributing to the enrichment of the transcription-associated ontologies included the transcription factors Ets2 and Jun, a known immediate-early gene product of the Mapk pathway.[32] The dual specificity phosphatases (Dusps) 4, 5, and 14, which are negative feedback regulators of the Mapk pathway, contributed to the enrichment of Map kinase phosphatase activity (Figure 4F; Table S17). In the lung and heart, several immune-associated processes were enriched within the top 5, including "immune receptor activity" in both (Figure 4F; Tables S18 and S19). While we cannot exclude the possibility that the presence of blood in both organs contributed to enrichment of this function, the fact that different genes contributed to its enrichment in each organ suggests that the enrichment was organ-specific, rather than blood-specific. We also noted "protein tyrosine kinase activator activity" in the top

Figure 4. Transcriptomic changes in response to Egf stimulation are tissue-specific

(A) PC1 versus PC3 from PCA of the RNA-seq dataset incorporating all treatment groups from all tissues. Colors represent each treatment group for each time point for each tissue.

(B) PC4 versus PC6 from PCA of the RNA-seq dataset incorporating al treatment groups from all tissues. Colors represent Egf-2 h, Egf-6 h, and no Egf treatment (incorporating all vehicle control and untreated samples).

(C) Volcano plots showing -$\log_{10}$(q-value) versus $\log_2$(fc) of gene expression following Egf stimulation in each tissue at 2 h (top) and 6 h (bottom). Significantly changed genes (FDR <5% and abs($\log_2$(fc)) > 1) are shown in red. Genes with an FDR <5% and abs($\log_2$(fc)) < 1 are shown in blue.

(D) UpSet plots comparing DEGs induced by Egf treatment in each tissue at 2 h and 6 h following Egf treatment.

(E) Comparison of the expression level of Egf-induced DEGs at 2 h (coral), 6 h (blue), and 2 h and 6 h (light green) following Egf treatment between the Egf-2 h and Egf-6 h treatment groups.

(F) Molecular function gene ontology analysis of Egf-induced DEGs at 2 h post-treatment in each tissue. Black boxes reflect the contribution of a given gene to a specific ontology.

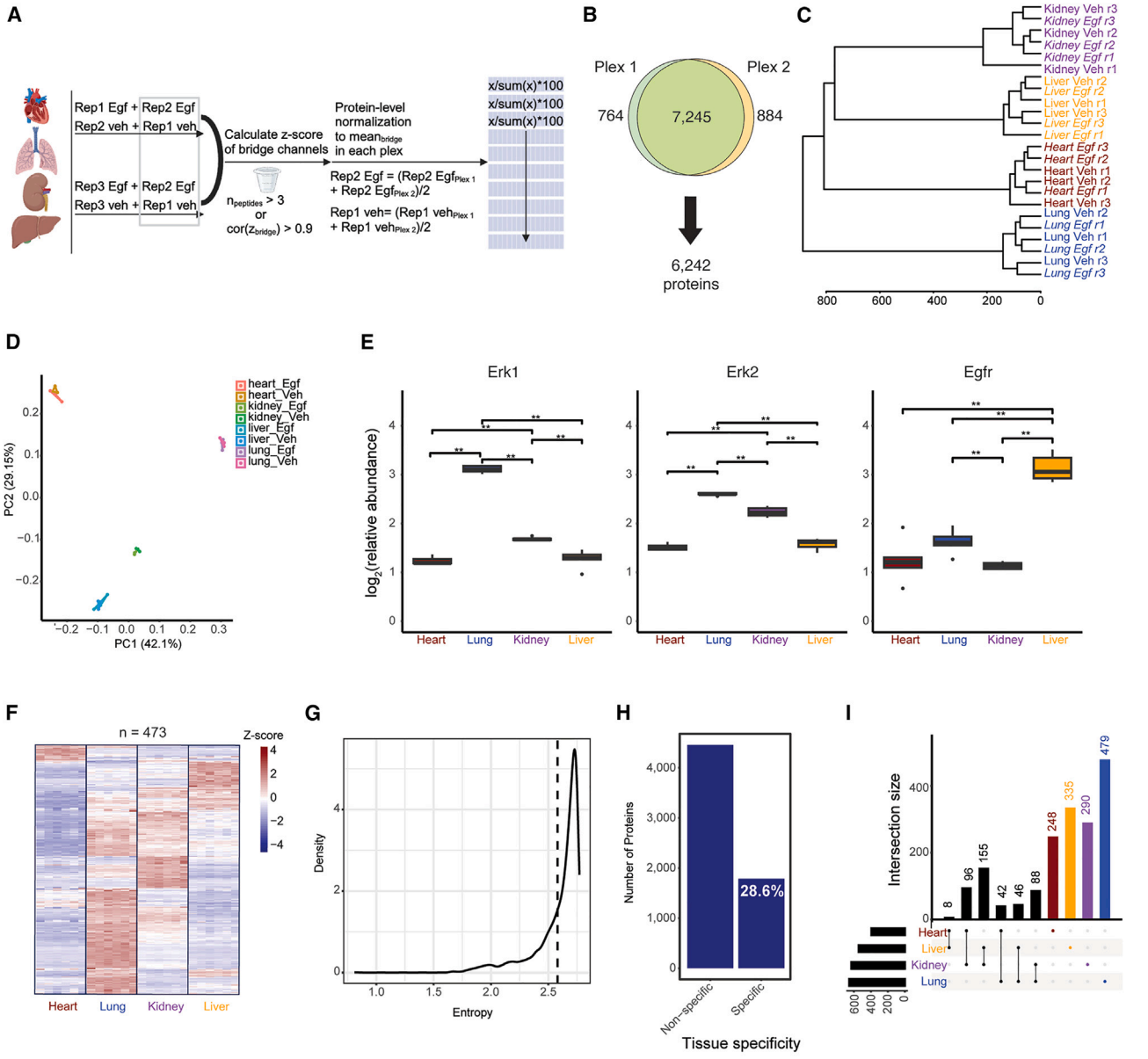

(legend on next page)

5 enriched molecular functions in the kidney and in the top 10 in the lung (Table S2, S18, and S20). Interestingly, the genes encoding the growth factors Hbegf and Nrg1 (which bind Egfr and Erbb4) contributed to its enrichment in both tissues, suggesting a common Egf-induced increase in growth factor signaling in the lung and kidney (Figure 4F; Tables S18 and S20). The gene encoding the Egfr ligand Areg additionally contributed to the "protein tyrosine kinase activator activity" enrichment in the lung (Table S18). In contrast, levels of Nrg1 transcripts, but not Hbegf or Areg, were significantly increased in the liver (Table S9). None of these transcripts were significantly increased in the heart (Table S11). Taken together, this analysis demonstrated substantial tissue specificity in the molecular functions associated with significant genes induced by Egf.

High Egfr, but not total protein levels of Egf-affected proteins, is linked to responsiveness to Egf

The phosphoproteomic and transcriptomic analyses of Egf-stimulated signaling within each tissue suggested that different tissues respond to Egf stimulation with different magnitudes of response and by the enrichment of distinct downstream molecular functions. We next focused on understanding the mechanisms by which tissues fine-tune their response to Egf. We hypothesized that one strategy for fine-tuning a tissue's response to Egf may be through modulating baseline total protein levels of the proteins involved in, or affected by, Egf stimulation. Additionally, tissues may exhibit a less robust induction of the pathway if the pathways are already active.

To be able to compare total protein levels of the Egfr and downstream pathway components across tissues, we prepared additional TMT experiments that included Egf-treated and control samples from each tissue within a single plex. This multiplexed design enabled us to directly compare total protein levels across tissues (Table S21). We used two TMT plexes to fit all the samples so that two Egf-treated and two vehicle control samples per tissue could be included in each plex. One replicate of each treatment and control sample for each tissue was included in both plexes to act as bridge channels. The total proteome was filtered to include proteins for which at least 3 peptides were detected or for which the Pearson correlation coefficient of the *Z* score of the bridge channels was greater than 0.9. Bridge-normalization within each TMT plex was performed using the mean of the bridge channels (Figure 5A). Filtering yielded 6,242 proteins in the bridge-normalized proteome (Figure 5B; Table S22). Tissues clustered together by both hierarchical clustering and PCA (Figures 5C and 5D), regardless of Egf treatment.

First, we compared the total level of Egfr across tissues relative to the total protein in the tissue. Notably, the liver had close to three times as much relative Egfr as the lung, which had the next highest relative level of Egfr of the four tissues (Figure 5E). This high relative level of Egfr could contribute to the high responsiveness of the liver to Egf stimulation. We also compared the total level of downstream proteins of Egfr signaling between tissues. Since the Erk proteins were commonly predicted to be the most activated kinases in response to Egf stimulation across tissues, we began by investigating the total protein levels of Erk1 and Erk2. In contrast to Egfr, the lung had significantly higher relative levels of both Erk1/2 than the other tissues (Figure 5E).

Additionally, we evaluated the relative levels of Egf-affected substrates—defined as proteins for which at least one phosphopeptide was significantly changed in response to Egf in at least one tissue in the individual tissue plexes—across tissues. In all, 473 Egf-affected substrates were detected in our multi-tissue plex. The total relative levels of most Egf-affected substrates were strikingly higher in the lung than in the other tissues, followed by the kidney (Figure 5F). Despite its high responsiveness to Egf, total relative levels of most Egf-affected proteins appeared lower in the liver than in the kidney and lung. Relative levels of Egfr, Erk1/2, and Egf-affected substrates were significantly lower in the heart than in the other tissues, consistent with its low responsiveness to Egf stimulation (Figures 5E and 5F).

Altogether, this analysis of total protein levels suggests a link between high total relative levels of Egfr—but not total effector or substrate protein levels—and the high responsiveness of the liver to stimulation of the Egfr. While the lung had the highest relative levels of downstream Egfr effector and substrate proteins of all tissues analyzed, these high relative levels did not appear to be the primary factor driving responsiveness to Egfr.

Significant Egf-affected proteins are disproportionately tissue-enriched in the lung

To investigate the association between total protein levels and phosphorylation in response to Egf more quantitatively, we

Figure 5. The liver has the highest total Egfr levels of all tissues, whereas the lung has higher levels of proteins in the Egf-stimulated phosphoproteome

(A) Schematic of multi-tissue TMT plexes and normalization strategy. The bridge samples are boxed. (Created with BioRender.com.).

(B) Total number of proteins detected in each TMT plex and the resulting number of proteins following filtering.

(C) Hierarchical clustering and (D) principal component analysis of the total proteome of each tissue following filtering and bridge-normalization. Egf-treated samples are shown in italics.

(E) Log_2(relative total abundance) of Erk1 (left), Erk2 (middle), and Egfr (right) in each tissue. Data are represented as log_2(relative abundance) within boxplots centered around the median of three replicates and whiskers extending to the upper and lower replicates. Significant differences between groups are marked with ** (Wilcoxon test, $p < 0.01$).

(F) Z-scores of total levels of proteins across tissues that were significantly changed in phosphorylation in at least one tissue in the individual tissue plexes. Z-scoring was performed across tissues using bridge-normalized total proteome dataset.

(G) Density plot of entropy distribution of total proteins across tissues. Proteins with entropy <2.58 (to the left of the dotted line) were deemed tissue-specific.

(H) Proportion of the total proteome that was tissue-specific versus not tissue-specific.

(I) Number of tissue-specific proteins detected in each tissue and combination of tissues.

(J) Proportion of proteins that were significantly ("sig") versus not significantly ("n.s.") altered in phosphorylation in response to Egf stimulation in each tissue that was tissue-specific versus not enriched. Conclusions about significant changes were derived from the individual tissue plexes.

subsequently used Shannon entropy[33] to assign each protein within the full tissue plex a tissue-specificity value and analyzed the proportion of Egf-affected and -unaffected proteins that were tissue-enriched. Shannon entropy has been previously used as a measure of the tissue specificity of proteins, where proteins with a low entropy value were deemed tissue-enriched, whereas proteins with a high entropy value were more ubiquitously expressed across tissues.[20] Here, proteins were defined as tissue-enriched if they had an entropy score less than 2.58, which corresponded to 80% of the signal of a given protein coming from two tissues (Figure 5G). Based on this calculation, approximately 28% of the proteins (n = 1787) in the multi-tissue experiment were deemed tissue-enriched (Figure 5H). Of these, the lung had the highest number of tissue-enriched proteins (Figure 5I).

In order to determine if Egf-stimulated proteins were more or less likely to be tissue-enriched, we focused on the proteins that were detected in both the single tissue and multi-tissue plexes. For each tissue, between 1,400 and 1,900 proteins were detected both in the individual tissue plexes and in the multi-tissue experiment; Egf-affected proteins were then defined within this analysis as those significantly changed by Egf stimulation in the single-tissue plexes. Strikingly, nearly 19% of Egf-affected proteins were tissue-enriched in the lung, whereas only 13% of the proteins not significantly changed in phosphorylation in response to Egf were lung-enriched. This contrasted with the heart, kidney, and liver, in which only 4%, 8%, and 6% of Egf-affected proteins, respectively, were tissue-enriched, while 12–14% of proteins that were not significantly affected by Egf were still tissue-enriched in each (Figure 5J). This analysis demonstrates that proteins significantly phosphorylated in response to Egf may have a higher propensity to be tissue-enriched in the lung than in other tissues. Furthermore, this finding was unlikely to be solely attributable to a higher overall proportion of tissue-enriched proteins in the lung than in other tissues, since the proportion of tissue-enriched proteins not significantly affected by Egf was similar across tissues.

Baseline phosphorylation levels of the Egf-stimulated phosphoproteome are highest in the lung

Given the high total levels of downstream Egfr effectors and substrates in the lung, we next asked whether these high levels were reflected in the baseline phosphoproteome (i.e., phosphorylation levels prior to Egf stimulation). To investigate this possibility, we prepared multi-tissue TMT experiments of the phosphoproteome to complement the total proteome multi-tissue plexes (Table S23). The phosphoproteome was filtered so that the correlation coefficient of the Z score of the bridge channels was greater than 0.9, and bridge-normalization within each TMT plex was performed as with the total proteome using the mean of the bridge channels. The two filtered and bridge-normalized TMT plexes were subsequently merged to yield a single multi-tissue phosphoproteomic dataset containing 3,017 phosphopeptides (Figure 6A; Table S24). Within this merged dataset, tissues clustered together by both hierarchical clustering and PCA. Within each tissue, most Egf-treated samples clustered separately from vehicle control samples, as well, with the exception of the heart (Figures 6B and 6C).

We first investigated the baseline phosphorylation levels of Erk1 and Erk2. The relative baseline phosphorylation levels of the Erk proteins were notably higher, though not significantly so, in the lung than in other tissues, reflecting higher relative intrinsic Mapk activity in the lung (Figure 6D). The lack of significance was likely due to the small sample size. Nevertheless, relative levels of pErk1 (Tyr205) were 2-fold higher in the lung than in the kidney, which had the next highest levels, and levels of pErk2 (Tyr185) were also highest in the lung. Relative baseline phosphorylation levels of Erk were lowest in the liver and heart, suggesting relatively low activation. The other two phosphorylation sites on the Erk proteins did not pass filtering criteria. Notably, relative phosphorylation of Egfr on the autophosphorylation site Tyr1172—whose phosphorylation contributes to activation of downstream effector pathways, including Mapk—was similar across tissues in the vehicle control-treated samples, indicating that relatively high Erk phosphorylation in the lung occurs in the context of comparable external receptor activation between tissues (Figure 6D).

Subsequently, we extended the analysis of baseline phosphorylation levels to the whole Egf-associated phosphoproteome. One limitation of the multi-tissue plex is the possible compression of the induced changes due to variability between tissues. Therefore, we used the single-tissue plex to first identify significantly Egf-affected phosphopeptides, which we analyzed in the multi-tissue plex. Of the 1,338 phosphopeptides that were significantly changed by Egf stimulation in at least one tissue, 215 were detected in the multi-tissue plex. Of these 215, the majority were found to have the highest baseline phosphorylation levels in the lung (Figure 6E, left heatmap). Very few were found at higher relative baseline levels in the liver and heart, with only slightly more in the kidney (Figure 6E, left heatmap). Together with the higher phospho-Erk levels in the lung, this analysis supported that the relative baseline Egf-associated phosphoproteome was, indeed, more active in the lung than in the other tissues. These observations also revealed a positive association between relative total protein levels and phosphorylation within the Egf-associated phosphoproteome. Specifically, the lung has the highest relative total protein and baseline phosphorylation of Egf-associated phosphopeptides, whereas the liver and heart have low relative total protein and baseline phosphorylation.

Following Egf stimulation, relative phosphorylation of Erk1 remained highest in the lung, despite comparatively higher phosphorylation increases in the kidney and liver (Figures 6F and 3B). Additionally, the relative phosphorylation of most Egf-affected phosphopeptides remained highest in the lung relative to the other stimulated tissues (Figure 6E). In contrast, relative phosphorylation of Egfr at its autophosphorylation site Tyr1172 rose to strikingly higher levels in the liver, which was consistent with the observed increase in Mapk activity (Figure 6F). Together, the phosphorylation patterns of Egf-affected peptides suggest that high baseline phosphorylation levels in the lung predispose the tissue to attaining higher levels of Egf signaling activity, even in the context of relatively lower magnitude phosphorylation fold-changes than the kidney and liver. Moreover, the high baseline phosphorylation of Egf-associated proteins

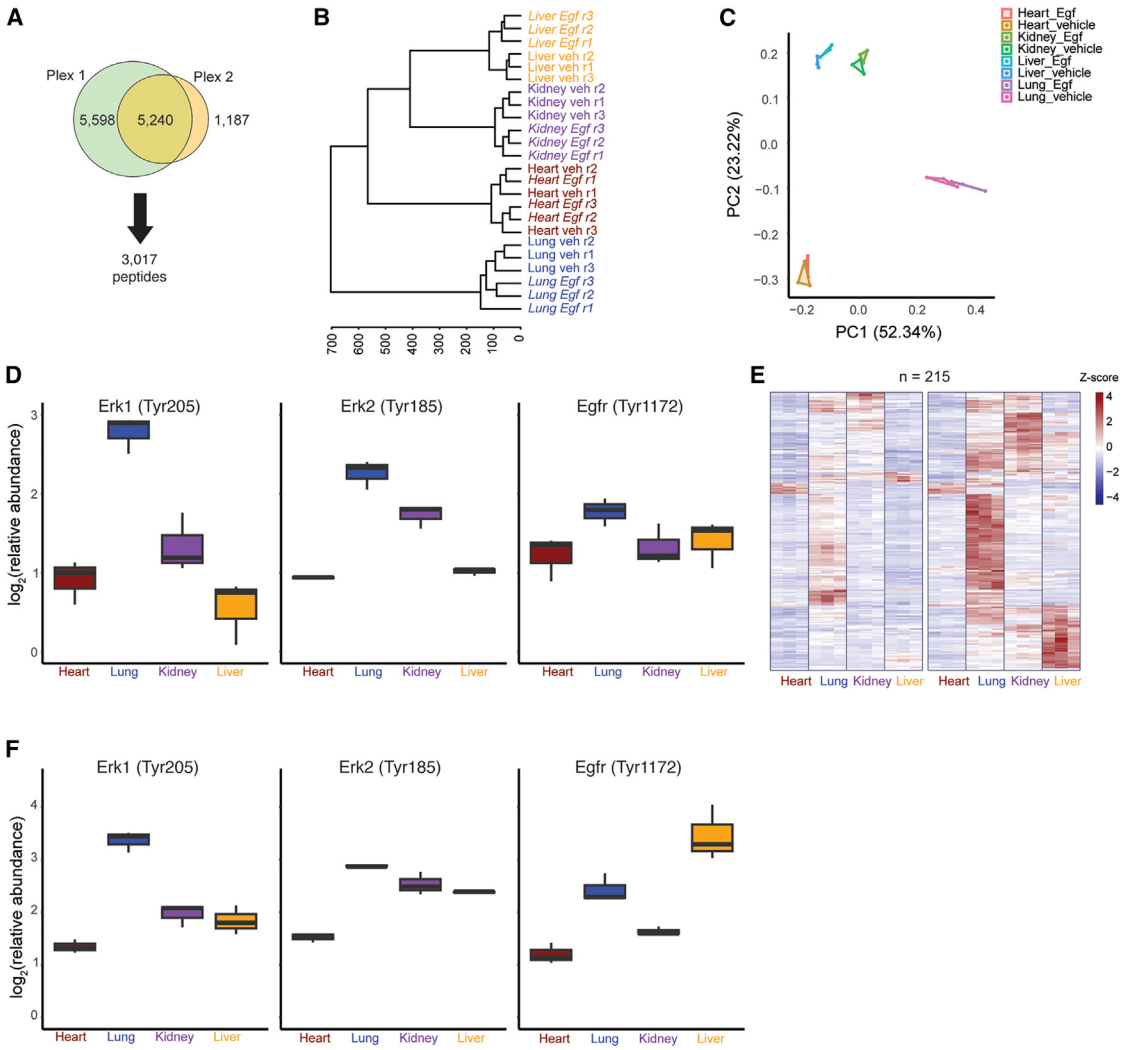

Figure 6. The lung has the highest baseline activity of the Egf-stimulated phosphoproteome

(A) Total number of phosphopeptides detected in each TMT plex and resulting number of proteins following filtering.

(B) Hierarchical clustering and (C) principal component analysis of the phosphoproteome of each tissue. Values used for clustering are normalized as shown in (A). Egf-treated samples are shown in italics.

(D) Log_2(relative abundance) of pErk1 (Tyr205) (left), pErk2 (Tyr185) (middle), and pEgfr (Tyr1172) (right) in the vehicle control-treated tissues. Data are represented as log_2(relative abundance) within boxplots centered around the median of three replicates and whiskers extending to the upper and lower replicates.

(E) Z scores of baseline phosphorylation levels (left) and Egf-stimulated phosphorylation levels (right) across tissues of phosphopeptides significantly affected by Egf stimulation in any tissue in the individual tissue plexes. Z-scoring was performed across tissues using the bridge-normalized phosphoproteomic dataset.

(F) Log_2(relative abundance) of pErk1 (Tyr205) (left), pErk2 (Tyr185) (middle), and pEgfr (Tyr1172) (right) in the Egf-treated tissues. Data are represented as log_2(relative abundance) within boxplots centered around the median of three replicates and whiskers extending to the upper and lower replicates.

appeared to be associated with high total protein levels but did not depend on external pathway activation. On the contrary, in the heart, in which there was a similar fold-change in Erk phosphorylation to that in the lung but notably lower baseline activation of the Egf-associated phosphoproteome, activation of downstream Egf-associated components following stimulation with Egf was much lower. Likewise, phosphorylation of most Egf-associated proteins in the liver following stimulation with Egf remained lower than in the lung, despite the relatively higher levels of Egfr phosphorylation and corresponding higher-magnitude response to Egf in the liver.

Linear mixed models quantify contribution of various factors to phosphorylation levels

Finally, we sought to quantitatively assess the relative contribution of external stimulation, intrinsic tissue biology, and total protein levels on the phosphorylation level of sites in our dataset. To that end, we fit linear mixed models to quantify the level of each phosphopeptide as a function of total protein level, Egf stimulation, tissue type, and replicate. The total protein level, Egf stimulation, and tissue type were included as fixed effects, while replicate was included as a random effect. We also included an additional fixed effect ‘‘interaction’’ term

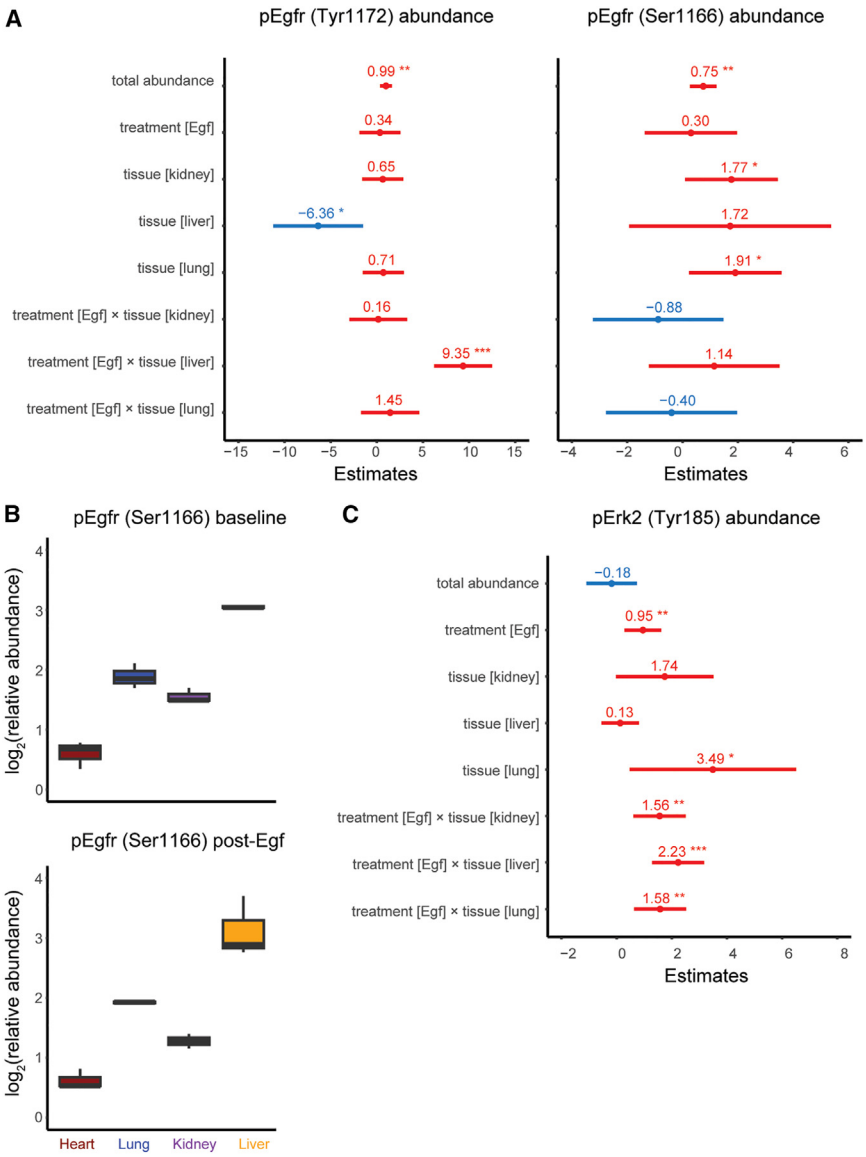

Figure 7. Linear mixed effects models reflect the relative association of Egf stimulation, tissue type, and total protein level with phosphorylation level

(A–C) Linear mixed effects models incorporating total protein level, tissue type, treatment, and the interaction between treatment and tissue type as fixed effects and replicate as a random effect were used to model levels of pEgfr (Tyr1172) and pEgfr (Ser1166) (A) and pErk2 (Tyr185) (C). Coefficients for each effect are shown, and significant coefficients are marked with **. (B) Log_2(relative abundance) of pEgfr (Ser1166) in vehicle control-treated samples (top) and with Egf-treated samples (bottom). Data are represented as log_2(relative abundance) within boxplots centered around the median of three replicates and whiskers extending to the upper and lower replicates.

to reflect the interaction between tissue type and Egf stimulation, reasoning that tissue type may play a unique role following Egf stimulation when compared to unstimulated tissues.

Using this strategy, we modeled the phosphorylation level of pEgfr (Tyr1172), pEgfr (Ser1166), and pErk2 (Tyr185). While Egfr has several phosphorylation sites, including multiple autophosphorylation sites, we restricted our study to pEgfr (Tyr1172) and pEgfr (Ser1166) to enable more in-depth comparison. The total protein level was predicted to contribute to phosphorylation of Egfr at Tyr1172, as indicated by the significant positive coefficient value (Figure 7A, left). Specifically in the liver, in the absence of stimulation with Egf, the coefficient for tissue type was negative, suggesting that repression of phosphorylation occurs in the liver at this site at baseline (Figure 7A, left). In contrast, upon Egf stimulation, the level of phosphorylated Tyr1172 in the liver was strikingly positively impacted, as indicated by the interaction term "treatment [Egf] x tissue [liver]". The coefficients for each variable were notably different for another Egfr phosphorylation site, Ser1166, for which total protein levels, lung, and kidney were significant contributors, but not liver (Figure 7A, right). This prediction is consistent with our earlier observations; Ser1166 was not highly phosphorylated in the liver in the single tissue plexes, and it appeared to be slightly decreased in response to Egf stimulation in the lung and kidney (Figure 1D). The coefficients in the model were also consistent with the relative levels of pEgfr (Ser1166) observed between tissues. Specifically, levels of pEgfr (Ser1166) were highest in the liver both pre- and post-Egf stimulation, which was in line with the liver having the highest total amount of Egfr (Figures 7B and 5E). Together, these contrasting Egfr phosphopeptides demonstrate that each phosphorylation site undergoes unique regulation and potentially has different roles in response to stimulation by Egf.

For pErk2 (Tyr185), total protein level was not predicted to play a significant role in phosphorylation. Rather, Egf stimulation, lung tissue type, and the interaction of Egf with the kidney, liver, and lung were significant contributors to the level of phosphorylation (Figure 7C). Here, the highly positive coefficient of the "lung" variable is consistent with the relatively higher baseline levels of pErk2 (Tyr185) in the lung than other tissues (Figure 6D), whereas the other significant variables reflect the effect of Egf in each tissue.

This model independently supports the idea that levels of certain phosphopeptides following Egf stimulation could be constrained primarily by total protein levels (such as for pEgfr (Ser1166)), whereas for others, total protein levels appear less

relevant. Furthermore, for some phosphopeptides (like pErk2 (Tyr185)), Egf alone is significantly associated with phosphorylation level across tissues, whereas for others, the significant association between Egf and phosphorylation level depends on tissue type (like pEgfr (Tyr1172)).

DISCUSSION

Egfr-driven signaling is central to fundamental cell processes in various tissues and the dysregulation of both Egfr- and effector pathway-driven signaling is implicated in several diseases. Despite numerous indications that these signaling pathways and their role in disease are highly tissue-specific, understanding of how Egfr-associated signaling processes compare between distinct tissues is limited. Here, we investigated tissue-specific responses to systemic short-term stimulation with the Egfr ligand Egf in the heart, lung, kidney, and liver of 10-week-old female mice. We integrated phosphoproteomic and transcriptomic analyses to study immediate phosphorylation changes within the Egf-driven phosphoproteome upon stimulation with one dose of Egf and short-term gene expression changes arising in the hours thereafter.

Using single-tissue TMT plexes, we found that Egf largely induced phosphorylation of the same phosphorylation sites between tissues, but that the magnitudes of the fold-changes in the global phosphoproteome were tissue-specific. Many Egf-affected substrates in our data were consistent with previously identified substrates *in vitro*.[34,35] Nevertheless, our finding that many substrates were only significantly phosphorylated in one tissue or a subset of tissues demonstrates the importance of studying *in vivo* signaling in multiple tissue contexts. Of the tissues we analyzed, the liver had the greatest magnitude of Egf-driven phosphoproteomic changes, while the heart had the lowest. One caveat to these experiments is the biodistribution of Egf following the retro-orbital injections. Although it is possible that each tissue received a different amount of Egf that could affect the magnitude of phosphorylation changes in response to Egf, our experiments demonstrate that all tissues induce signaling changes; for example, the increase in phosphorylation of Egfr and Erk confirms that Egf stimulation had an effect in the four tissues chosen (Figures 1D and 3B). In contrast to these four tissues, phosphoproteomic analysis of the brain showed no significant response to Egf (data not shown), which is consistent with the previous observations that Egf cannot cross the blood-brain barrier. This finding in the brain additionally supports that phosphorylation changes observed in our experiment were truly due to Egf stimulation.

Proteins with significantly altered phosphorylation changes were enriched for cytoskeleton and other structure-associated gene ontologies in all tissues. The significant proteins in the liver and kidney, which had the second highest number of significant phosphorylation changes in response to Egf stimulation, were additionally enriched for transcription and DNA binding-associated functions, indicating a potential association between the magnitude of phosphoproteomic changes and Egf-affected transcriptional functions within tissues. In the lung, Egf-affected proteins were additionally enriched for GTPase-regulating activities. Consistent with our findings in the kidney and liver, previous analysis of the gene ontologies of Egf-induced proteins in HeLa cells, likewise, revealed induction of cytoskeletal and transcriptional ontologies.[34] Additionally, substantial phosphorylation of GTPase-interacting proteins was noted in response to Egf stimulation in the HeLa cells, which was in line with our findings in the lung. The observation that distinct combinations of these previously reported Egf-affected ontologies were enriched among Egf-affected proteins in different tissue contexts was notable and further supports the idea that tissue context is essential when considering the effects of Egf signaling in physiological contexts.

Activation of the Mapk pathway was a shared response to Egfr activation across all tissues. Of note, although gene ontologies that were enriched among the Mapk-dependent Egf-regulated phosphoproteins were similar across tissues, the proportion of significant Egf-affected phosphopeptides that were Mapk-dependent appeared to vary between tissues. Therefore, the Mapk pathway may regulate similar functions in response to Egf stimulation across tissues, although the relative proportion of significant Mapk-regulated phosphosites in response to Egf among all significantly Egf-affected sites within a tissue may be tissue-specific.

At the same time, the activation of other downstream Egfr effector pathways was much less uniform across tissues. Remarkably, we did not observe comparable activation of the PI3K/Akt pathway based on phosphorylation of known activating peptides within the pathway, and in fact, mTOR activity was predicted by kinase enrichment analysis to be significantly downregulated in the lung in response to Egf. We did note tissue-specific significant phosphorylation changes on Stat family proteins, another Egfr effector family. For instance, phosphorylation of the Egfr effector Stat5b at its activating site S699 was significantly increased after Egf treatment, especially in the presence of Meki, in the lung, whereas it was not significantly changed in any condition in the kidney (Tables S4 and S6). Kinase inhibitor studies would be necessary for more in-depth studies of these other effector pathways. Given the relative sparsity of phosphopeptides in these pathways detected relative to phosphopeptides within the Mapk pathway, we did not pursue further study. Nevertheless, our observations suggest that that Egf may lead to different extents of activation of other non-MAPK effector pathways between tissues. Different combinations of pathway activation may also contribute to tissue-specific responses to Egf stimulation and would warrant further exploration.

At the transcriptomic level, the liver had the highest number of significant gene expression changes, followed by the lung, heart, and kidney. Several known immediate-early gene (IEG) targets of the Mapk pathway were detected across tissues at 2 h post-Egf stimulation, including the Egr family members (heart), cFos (lung), and Jun (liver). Mapk-stimulated IEG targets have been well-studied and are known to be enriched for transcription-associated functions that, upon repeated Mapk stimulation, eventually drive gene expression changes.[32,36] Consistent with these studies, Egf-stimulated DEGs at 2 h post-stimulation in the liver were enriched in transcription-associated processes among the top 5 enriched molecular functions. While these ontologies were not included in the top enriched molecular

functions in the other tissues, expression of individual IEGs was increased, nonetheless. We also observed increased expression of the Dusp transcripts, most significantly in the liver. These phosphatases negatively regulate the Mapk pathway by dephosphorylating the Erk proteins and are additional known early gene targets of activated Mapk.[37] Thus, our transcriptomic analyses were consistent with the phosphoproteome in suggesting that Mapk signaling was activated by Egf stimulation across tissues. Nevertheless, there was strikingly little overlap between the significant DEGs induced by Egf between tissues, demonstrating a high degree of tissue specificity at the transcriptome level, as well.

Interestingly, PCA indicated that the transcriptomic response to Egf stimulation varied dramatically between time points post-stimulation (e.g., 2 h versus 6 h). This finding is consistent with the observation that genes upregulated at 2 h post-Egf treatment had, for the most part, returned to baseline by 6 h, whereas the genes increased at the 6 h time point had not yet increased at 2 h. The timing of gene expression changes regulated by the Mapk pathway has been well-studied. Specifically, it is known that, in addition to immediate-early genes, there are several other distinct groups of Mapk-regulated genes—immediate-late, delayed-response, and secondary-response genes—with unique functional and temporal expression characteristics.[32,36] In this analysis, the genes expressed at 2 h likely represent a combination of immediate-early and immediate-late genes, while the genes expressed at 6 h may contain a higher proportion of delayed-response and secondary-response genes. Of note, it is likely that the differential expression of some immediate-early genes was not detected in this experiment because these genes are expressed within minutes following Mapk stimulation, meaning that their expression may have already declined to levels below our significance threshold by the 2-h time point.

Within the multi-tissue TMT plexes for the total proteome, we detected significantly higher relative levels of Egfr in the liver compared to other tissues, which was consistent with previous studies,[38] but notably higher relative levels of most Mapk components and Egf-affected proteins in the lung. This observation suggested that high relative levels of Egfr—but not downstream proteins—are associated with responsiveness to stimulation with Egf. Remarkably, despite the significantly higher total relative Egfr levels in the liver, the relative abundance of the phosphopeptide pEgfr (Tyr1172) was similar across all tissues in the absence of Egf stimulation. Tyr1172 is a known autophosphorylation site of Egfr involved in stimulation of Ras/Mapk signaling, Upon stimulation with Egf, phosphorylation of this site increased to more than 2-fold higher relative levels in the liver than in any other tissue. In agreement with this observation, in a linear mixed model evaluating the contribution of the total protein level, tissue type, treatment type, and interaction between tissue type and treatment type to pEgfr (Tyr1172) levels, the coefficient for baseline liver was significantly negative, whereas the coefficient for the interaction between liver and Egf treatment was significantly positive. The coefficient for total abundance was also positive. The significant positive coefficient for the interaction between liver and Egf treatment further implied that the liver has high potential for responsiveness to stimulation with Egf in the context of phosphorylation of pEgfr at Tyr1172. Given that this phosphorylation site participates in Ras/Mapk signaling, its high responsiveness to stimulation with Egf is consistent with the high magnitudes of Ras/Mapk-associated phosphoproteomic and transcriptomic changes observed in the liver in response to Egf stimulation. Moreover, the significantly negative coefficient of baseline liver in the model of pEgfr (Tyr1172) levels suggested that this high potential for Egf-driven signaling may be relatively suppressed in the absence of stimulation. Therefore, high total relative Egfr protein levels, in conjunction with carefully regulated phosphorylation of Tyr1172 residue, may contribute to the high potential of the liver for responsiveness to stimulation with Egf.

Conversely, the higher total relative protein levels of downstream effector proteins of the Egfr were associated with greater phosphorylation within the Egf-associated phosphoproteome of the lung both at baseline and following Egf stimulation, despite a lower magnitude of phosphoproteomic and transcriptomic changes in response to stimulation than the liver. Of note, the higher relative baseline phosphorylation of the Egf-associated phosphoproteome was not associated with higher relative Egfr phosphorylation, supporting the conclusion that the phosphorylation was internally driven. Taken together, these data suggested that the lung has a relatively more active Egf-associated phosphoproteome than the liver, kidney, and heart at baseline. As discussed earlier, the development of many human cancers of the lung is known to be driven by mutations in *EGFR*, *KRAS*, and *BRAF*, and these mutations occur much more frequently in cancers of the lung than in the other three tissues.[39] This high baseline relative activity and total protein level of Egf effectors could play a role in the increased susceptibility of the lung to oncogenic mutations in these genes. Specifically, a smaller increase in Egfr-associated activity may be sufficient to push the lung into a pro-proliferative, pro-growth state. In contrast, the heart, which has low relative levels of baseline Egf phosphoproteomic, proteomic, and transcriptomic activity, would likely require a much greater boost in Egfr activity to achieve any proliferation. Consistent with this possibility, the heart has low known proliferative activity.[25]

It is important to note that Egfr signals as a dimer, either as a homodimer or within a heterodimer with ErbB2 or ErbB3, and that levels of these other proteins may also affect the tissue-specific outputs of Egf stimulation described here.[40,41] Additionally, the behavior of other ligands and receptor tyrosine kinases may influence signaling patterns within each tissue. Egfr dimerization patterns and other receptor tyrosine kinases are complex and warrant a separate study that is beyond the scope of this work. We found that some receptors could not be detected in our bulk proteomic/phosphoproteomic dataset, meaning that targeted mass spectrometry approaches may be needed to reliably detect all receptors of interest. Nevertheless, specific study of dimerization patterns would likely provide a valuable extra layer in understanding the intricacies of tissue-specific Egf-driven signaling. Likewise, phosphatases play an important role in dephosphorylating both Egfr and various downstream effector proteins.[42] Due to the intricate nature of the assembly and disassembly of subunits of many phosphatase families and their crucial role in substrate specificity,[43,44] their specific study requires a more nuanced and focused approach than the broad omics studies discussed here, ideally using phosphatase

inhibitors and more targeted examples. For analysis of the effect of phosphatase activities on Egfr activity in cells, we reference other work that has been performed specifically with this focus.[45] Finally, Egfr interfaces with several adapter proteins, which bind to various phosphorylation sites on Egfr that were not discussed in-depth here.[46] While we were unable to address all of these within this single piece, their future study would also enhance understanding of Egfr signaling.

Altogether, results of this study demonstrate that different tissues have unique profiles of Egf-driven signaling. Moreover, we showed that a distinction can be made between the level of baseline Egf-associated signaling and responsiveness to Egf-stimulated signaling when considering Egf-driven signaling between tissues. The levels of both baseline and stimulation-driven Egf-associated signaling define the behavior of tissues in the context of Egf-associated effects. Additionally, when considering the effects of Egf stimulation within a given tissue, the magnitudes of phosphoproteomic and transcriptomic changes might differ within a tissue, as seen in the kidney, which had relatively high phosphoproteomic changes compared with the other tissues, but the fewest transcriptomic changes. Finally, given that the baseline levels of Egf-associated proteins and phosphoproteins are notably different between tissues, it is possible that different magnitudes of fold-changes could elicit distinct effects between tissues, depending on the baseline levels. Understanding the key characteristics of the Egf-associated signaling profile within each tissue could aid in modulating Egf and Egfr-based treatment strategies for various tissue-specific conditions. For instance, better understanding of the factors that repress Egf-associated signaling in the heart could help attenuate the pathway in the lung in cases of disease pathology driven by hyperactive Egf-associated signaling. Likewise, understanding the drivers of the high baseline Egf-associated signaling pathways in the lung and the high responsiveness of the liver to Egf stimulation could give insight into how to modulate Egf-driven proliferation in the heart. Linear mixed modeling to understand factors associated with phosphorylation levels as described in this work for Egfr (Tyr1172 and Ser1166) and Erk (Tyr185) could be applied to other phosphorylation sites to generate hypotheses for further experiments in this vein.

Limitations of the study

Since the experiments described here were performed in bulk tissue samples, rather than single cells, these data do not provide insight into cell-type specific contributions to Egf-stimulated tissue behavior. Future single-cell transcriptomic analysis, in combination with spatial profiling, could provide insight into the mechanisms by which different cell types within each tissue work together to carry out Egf-stimulated behaviors. Additionally, since we evaluated Egf-induced signaling at short time points after a single bolus of Egf, signaling changes and consequent phenotypic changes induced by more sustained exposure to Egf remain largely unresolved. Mice engineered to chronically express higher levels could be employed to conduct similar signaling studies of long-term Egf exposure. Finally, future studies should be conducted to evaluate the role of other ErbB family proteins, Egf family ligands, and adaptor proteins in Egfr signaling.

RESOURCE AVAILABILITY

Lead contact

Further information and requests for reagents should be directed to the lead contact, Kevin M. Haigis (kevin_haigis@dfci.harvard.edu).

Materials availability

There are no unique materials generated from this study.

Data and code availability

- Processed data, including calculated fold-changes from transcriptomic and proteomic data, are available in Supplementary Tables. Additional details can be provided by the lead contact.
- Raw data for gene expression analyses have been deposited into NCBI GEO (Accession number: GSE262676). Raw data for proteomic analyses have been deposited into ProteomeXchange (Dataset identifier: PXD050402). Accession numbers are available in the key resources table. All custom code has been deposited to GitHub (https://github.com/Beawasthi/Egf-signaling).
- All software used for analysis have been described in the key resources table. Additional details can be provided by the lead contact.

ACKNOWLEDGMENTS

Thank you to Professors Peter Sicinski and Kamila Naxerova and to all the members of the Haigis lab, especially Dr. Olesja Popow, for their feedback. This work was supported by an award from the Cancer Research UK Grand Challenge and the Mark Foundation to the SPECIFICANCER team. B.W.A. was supported by the Landry Cancer Biology Research Fellowship. RNA-sequencing and mapping to the transcriptome were performed by Novogene. J.W.H. was supported by NIH grant AG011085. Some figures were generated using BioRender.com.

AUTHOR CONTRIBUTIONS

This study was conceptualized by B.W.A. and K.M.H. J.A.P. and D.L.B. consulted on conceptualization. B.W.A. performed all sample preparation for mass spectrometry and RNA-sequencing experiments and the majority of the bioinformatic analyses. J.A.P. oversaw all mass spectrometers. D.L.B and B.W.A. performed all animal experiments. I.R.S. wrote scripts for MSstatsPTM analysis. R.L.C. consulted on computational analyses. B.W.A. and J.A.P. performed data curation. B.W.A., J.A.P, and K.M.H. wrote the original manuscript and J.A.P., D.L.B., I.R.S., and R.L.C. participated in review and editing. J.W.H., S.P.G., and K.M.H. supervised.

DECLARATION OF INTERESTS

J.W.H. is a consultant and founder of Caraway Therapeutics (a wholly owned subsidiary of Merck & Co, Inc) and is a member of the scientific advisory board for Lyterian Therapeutics.

STAR★METHODS

Detailed methods are provided in the online version of this paper and include the following:

- KEY RESOURCES TABLE
- EXPERIMENTAL MODEL AND STUDY PARTICIPANT DETAILS
  - Animal models
- METHOD DETAILS
  - Mouse treatments and tissue collection
  - Sample preparation for phosphoproteomics/proteomics
  - Offline basic pH reversed-phase (BPRP) fractionation for whole proteome TMT-based experiment
  - Mass spectrometry data acquisition
- QUANTIFICATION AND STATISTICAL ANALYSIS
  - Mass spectrometry data analysis

- Normalization and filtering of single-tissue TMT plexes
- Kinase enrichment analysis
- Significance analysis of phosphorylation changes within single tissue plexes
- Correlation of fold-changes calculated by MSstatsPTM versus in-house software in single-tissue plexes
- Gene ontology analysis for phosphoproteome
- Normalization of multi-tissue TMT plexes
- Shannon entropy analysis
- Linear mixed models
- RNA-seq library preparation
- mRNA quality control and read alignment
- mRNA differential expression analysis
- Gene ontology analysis for transcriptome
- Hierarchical clustering analysis
- Principal component analysis
- Volcano plots
- UpSet plots

SUPPLEMENTAL INFORMATION

Supplemental information can be found online at https://doi.org/10.1016/j.isci.2025.112146.

Received: April 22, 2024
Revised: July 29, 2024
Accepted: February 27, 2025
Published: March 4, 2025

REFERENCES

1. Natarajan, A., Wagner, B., and Sibilia, M. (2007). The EGF receptor is required for efficient liver regeneration. Proc. Natl. Acad. Sci. USA *104*, 17081–17086.
2. Tang, J., Liu, N., and Zhuang, S. (2013). Role of epidermal growth factor receptor in acute and chronic kidney injury. Kidney Int. *83*, 804–810.
3. Crosby, L.M., and Waters, C.M. (2010). Epithelial repair mechanisms in the lung. Am. J. Physiol. Lung Cell. Mol. Physiol. *298*, L715–L731.
4. Michalopoulos, G.K., and Bhushan, B. (2021). Liver regeneration: biological and pathological mechanisms and implications. Nat. Rev. Gastroenterol. Hepatol. *18*, 40–55.
5. Kumar, S. (2018). Cellular and molecular pathways of renal repair after acute kidney injury. Kidney Int. *93*, 27–40.
6. Berasain, C., and Avila, M.A. (2014). The EGFR signalling system in the liver: from hepatoprotection to hepatocarcinogenesis. J. Gastroenterol. *49*, 9–23.
7. Bierman, A., Yerrapureddy, A., Reddy, N.M., Hassoun, P.M., and Reddy, S.P. (2008). EGF receptor regulates mechanical ventilation induced lung injury in mice. Transl. Res. *152*, 265–272.
8. Yoshioka, J., Prince, R.N., Huang, H., Perkins, S.B., Cruz, F.U., MacGillivray, C., Lauffenburger, D.A., and Lee, R.T. (2005). Cardiomyocyte hypertrophy and degradation of connexin43 through spatially restricted autocrine/paracrine heparin-binding EGF. Proc. Natl. Acad. Sci. USA *102*, 10622–10627.
9. Harskamp, L.R., Gansevoort, R.T., van Goor, H., and Meijer, E. (2016). The epidermal growth factor receptor pathway in chronic kidney diseases. Nat. Rev. Nephrol. *12*, 496–506.
10. Foster, S.A., Klijn, C., and Malek, S. (2016). Tissue-Specific Mutations in BRAF and EGFR Necessitate Unique Therapeutic Approaches. Trends Cancer *2*, 699–701.
11. Schneider, G., Schmidt-Supprian, M., Rad, R., and Saur, D. (2017). Tissue-specific tumorigenesis – Context matters. Nat. Rev. Cancer *17*, 239–253.
12. Crombet Ramos, T., Santos Morales, O., Dy, G.K., León Monzón, K., and Lage Dávila, A. (2021). The Position of EGF Deprivation in the Management of Advanced Non-Small Cell Lung Cancer. Front. Oncol. *11*, 639745.
13. DeWitt, A., Iida, T., Lam, H.Y., Hill, V., Wiley, H.S., and Lauffenburger, D.A. (2002). Affinity regulates spatial range of EGF receptor autocrine ligand binding. Dev. Biol. *250*, 305–316.
14. Joslin, E.J., Shankaran, H., Opresko, L.K., Bollinger, N., Lauffenburger, D.A., and Wiley, H.S. (2010). Structure of the EGF receptor transactivation circuit integrates multiple signals with cell context. Mol. Biosyst. *6*, 1293–1306.
15. Pan, C., Olsen, J.V., Daub, H., and Mann, M. (2009). Global effects of kinase inhibitors on signaling networks revealed by quantitative phosphoproteomics. Mol. Cell. Proteomics *8*, 2796–2808.
16. Ünal, E.B., Uhlitz, F., and Blüthgen, N. (2017). A compendium of ERK targets. FEBS Lett. *591*, 2607–2615.
17. Fuchs, B.C., Hoshida, Y., Fujii, T., Wei, L., Yamada, S., Lauwers, G.Y., McGinn, C.M., DePeralta, D.K., Chen, X., Kuroda, T., et al. (2014). EGFR inhibition attenuates liver fibrosis and development of hepatocellular carcinoma. Hepatol. Baltim. Md *59*, 1577–1590.
18. Mancini, M., Thomas, Q.D., Bourdel, S., Papon, L., Bousquet, E., Jalta, P., La Monica, S., Travert, C., Alfieri, R., Quantin, X., et al. (2021). Generation and Characterization of a New Preclinical Mouse Model of EGFR-Driven Lung Cancer with MET-Induced Osimertinib Resistance. Cancers *13*, 3441.
19. Richards, W.G., Sweeney, W.E., Yoder, B.K., Wilkinson, J.E., Woychik, R.P., and Avner, E.D. (1998). Epidermal growth factor receptor activity mediates renal cyst formation in polycystic kidney disease. J. Clin. Investig. *101*, 935–939.
20. Huttlin, E.L., Jedrychowski, M.P., Elias, J.E., Goswami, T., Rad, R., Beausoleil, S.A., Villén, J., Haas, W., Sowa, M.E., and Gygi, S.P. (2010). A tissue-specific atlas of mouse protein phosphorylation and expression. Cell *143*, 1174–1189.
21. Melé, M., Ferreira, P.G., Reverter, F., DeLuca, D.S., Monlong, J., Sammeth, M., Young, T.R., Goldmann, J.M., Pervouchine, D.D., Sullivan, T.J., et al. (2015). The human transcriptome across tissues and individuals. Science *348*, 660–665.
22. Zhou, J., Sears, R.L., Xing, X., Zhang, B., Li, D., Rockweiler, N.B., Jang, H.S., Choudhary, M.N.K., Lee, H.J., Lowdon, R.F., et al. (2017). Tissue-specific DNA methylation is conserved across human, mouse, and rat, and driven by primary sequence conservation. BMC Genom. *18*, 724.
23. Kaza, A.K., Laubach, V.E., Kern, J.A., Long, S.M., Fiser, S.M., Tepper, J.A., Nguyen, R.P., Shockey, K.S., Tribble, C.G., and Kron, I.L. (2000). Epidermal growth factor augments postpneumonectomy lung growth. J. Thorac. Cardiovasc. Surg. *120*, 916–921.
24. Glanemann, M., Shi, B., El-Zidy, N., Gaebelein, G., Kronbach, Z., Neuhaus, P., and Nussler, A.K. (2009). Subcutaneous administration of epidermal growth factor: A true treatment option in case of postoperative liver failure? Int. J. Surg. *7*, 200–205.
25. Hesse, M., Welz, A., and Fleischmann, B.K. (2018). Heart regeneration and the cardiomyocyte cell cycle. Pflugers Arch. *470*, 241–248.
26. Michalopoulos, G.K. (2010). Liver regeneration after partial hepatectomy: critical analysis of mechanistic dilemmas. Am. J. Pathol. *176*, 2–13.
27. Martinez-Val, A., Bekker-Jensen, D.B., Steigerwald, S., Koenig, C., Østergaard, O., Mehta, A., Tran, T., Sikorski, K., Torres-Vega, E., Kwasniewicz, E., et al. (2021). Spatial-proteomics reveals phospho-signaling dynamics at subcellular resolution. Nat. Commun. *12*, 7113.
28. Navarrete-Perea, J., Yu, Q., Gygi, S.P., and Paulo, J.A. (2018). A Streamlined Protocol for Quantitative (Phospho)proteome Profiling using TMT-SPS-MS3. J. Proteome Res. *17*, 2226–2236.
29. Kohler, D., Tsai, T.H., Verschueren, E., Huang, T., Hinkle, T., Phu, L., Choi, M., and Vitek, O. (2023). MSstatsPTM: Statistical Relative Quantification of Posttranslational Modifications in Bottom-Up Mass Spectrometry-Based Proteomics. Mol. Cell. Proteomics *22*, 100477.

30. Johnson, J.L., Yaron, T.M., Huntsman, E.M., Kerelsky, A., Song, J., Regev, A., Lin, T.Y., Liberatore, K., Cizin, D.M., Cohen, B.M., et al. (2023). An atlas of substrate specificities for the human serine/threonine kinome. Nature *613*, 759–766.

31. Bogdan, S., and Klämbt, C. (2001). Epidermal growth factor receptor signaling. Curr. Biol. *11*, R292–R295.

32. Tullai, J.W., Schaffer, M.E., Mullenbrock, S., Sholder, G., Kasif, S., and Cooper, G.M. (2007). Immediate-Early and Delayed Primary Response Genes Are Distinct in Function and Genomic Architecture. J. Biol. Chem. *282*, 23981–23995.

33. Shannon, C.E. (1948). A mathematical theory of communication. Bell Syst. Tech. J. *27*, 379–423.

34. Olsen, J.V., Blagoev, B., Gnad, F., Macek, B., Kumar, C., Mortensen, P., and Mann, M. (2006). Global, In Vivo, and Site-Specific Phosphorylation Dynamics in Signaling Networks. Cell *127*, 635–648.

35. PhosphoSitePlus. https://www.phosphosite.org/homeAction.action.

36. Uhlitz, F., Sieber, A., Wyler, E., Fritsche-Guenther, R., Meisig, J., Landthaler, M., Klinger, B., and Blüthgen, N. (2017). An immediate–late gene expression module decodes ERK signal duration. Mol. Syst. Biol. *13*, 944.

37. Lake, D., Corrêa, S.A.L., and Müller, J. (2016). Negative feedback regulation of the ERK1/2 MAPK pathway. Cell. Mol. Life Sci. *73*, 4397–4413.

38. Komposch, K., and Sibilia, M. (2015). EGFR Signaling in Liver Diseases. Int. J. Mol. Sci. *17*, 30.

39. Gao, J., Aksoy, B.A., Dogrusoz, U., Dresdner, G., Gross, B., Sumer, S.O., Sun, Y., Jacobsen, A., Sinha, R., Larsson, E., et al. (2013). Integrative analysis of complex cancer genomics and clinical profiles using the cBioPortal. Sci. Signal. *6*, pl1.

40. Arteaga, C.L., and Engelman, J.A. (2014). ERBB receptors: From oncogene discovery to basic science to mechanism-based cancer therapeutics. Cancer Cell *25*, 282–303.

41. (2017). ErbB Receptor Signaling: Methods and Protocols*1652* (New York, NY: Springer New York).

42. Stanoev, A., Mhamane, A., Schuermann, K.C., Grecco, H.E., Stallaert, W., Baumdick, M., Brüggemann, Y., Joshi, M.S., Roda-Navarro, P., Fengler, S., et al. (2018). Interdependence between EGFR and Phosphatases Spatially Established by Vesicular Dynamics Generates a Growth Factor Sensing and Responding Network. Cell Syst. *7*, 295–309.e11.

43. Lyons, S.P., Greiner, E.C., Cressey, L.E., Adamo, M.E., and Kettenbach, A.N. (2021). Regulation of PP2A, PP4, and PP6 holoenzyme assembly by carboxyl-terminal methylation. Sci. Rep. *11*, 23031.

44. Haanen, T.J., 3rd, O'Connor, C.M., O'Connor, C.M., and Narla, G. (2022). Biased holoenzyme assembly of protein phosphatase 2A (PP2A): From cancer to small molecules. J. Biol. Chem. *298*, 102656.

45. Eguchi, A., and Olsen, J.V. (2024). Phosphoproteomic Investigation of Targets of Protein Phosphatases in EGFR Signaling. Sci. Rep. *14*, 7908. https://doi.org/10.1101/2024.02.01.578427.

46. Wee, P., and Wang, Z. (2017). Epidermal Growth Factor Receptor Cell Proliferation Signaling Pathways. Cancers *9*, 52.

47. Conway, J.R., Lex, A., and Gehlenborg, N. (2017). UpSetR: an R package for the visualization of intersecting sets and their properties. Bioinforma. Oxf. Engl. *33*, 2938–2940.

48. Chen, H., and Boutros, P.C. (2011). VennDiagram: a package for the generation of highly-customizable Venn and Euler diagrams in R. BMC Bioinf. *12*, 35.

49. Wu, T., Hu, E., Xu, S., Chen, M., Guo, P., Dai, Z., Feng, T., Zhou, L., Tang, W., Zhan, L., et al. (2021). clusterProfiler 4.0: A universal enrichment tool for interpreting omics data. Innovation *2*, 100141.

50. Love, M.I., Huber, W., and Anders, S. (2014). Moderated estimation of fold change and dispersion for RNA-seq data with DESeq2. Genome Biol. *15*, 550.

51. Kohler, D., Staniak, M., Tsai, T.H., Huang, T., Shulman, N., Bernhardt, O.M., MacLean, B.X., Nesvizhskii, A.I., Reiter, L., Sabido, E., et al. (2023). MSstats Version 4.0: Statistical Analyses of Quantitative Mass Spectrometry-Based Proteomic Experiments with Chromatography-Based Quantification at Scale. J. Proteome Res. *22*, 1466–1482.

52. Huang, T., Choi, M., Tzouros, M., Golling, S., Pandya, N.J., Banfai, B., Dunkley, T., and Vitek, O. (2020). MSstatsTMT: Statistical Detection of Differentially Abundant Proteins in Experiments with Isobaric Labeling and Multiple Mixtures. Mol. Cell. Proteomics *19*, 1706–1723.

53. Galili, T. (2015). dendextend: an R package for visualizing, adjusting and comparing trees of hierarchical clustering. Bioinforma. Oxf. Engl. *31*, 3718–3720.

54. Bates, D., Mächler, M., Bolker, B., and Walker, S. (2015). Fitting Linear Mixed-Effects Models Using lme4. J. Stat. Softw. *67*, 1–48.

55. Kuznetsova, A., Brockhoff, P.B., and Christensen, R.H.B. (2020). lmerTest Package: Tests in Linear Mixed Effects Models. J. Stat. Softw. *82*, 1–26.

56. Tang, Y., Horikoshi, M., and Li, W. (2016). ggfortify: Unified Interface to Visualize Statistical Results of Popular R Packages. R J. *8*, 474–485.

57. Ahlmann-Eltze, C., and Patil, I. (2021). ggsignif: R Package for Displaying Significance Brackets for 'ggplot2'. PsyArxiv. https://doi.org/10.31234/osf.io/7awm6.

58. Yu, G., Wang, L.-G., Yan, G.-R., and He, Q.-Y. (2015). DOSE: an R/Bioconductor package for disease ontology semantic and enrichment analysis. Bioinforma. Oxf. Engl. *31*, 608–609.

59. Chambers, M.C., Maclean, B., Burke, R., Amodei, D., Ruderman, D.L., Neumann, S., Gatto, L., Fischer, B., Pratt, B., Egertson, J., et al. (2012). A cross-platform toolkit for mass spectrometry and proteomics. Nat. Biotechnol. *30*, 918–920.

60. Wang, Y., Yang, F., Gritsenko, M.A., Wang, Y., Clauss, T., Liu, T., Shen, Y., Monroe, M.E., Lopez-Ferrer, D., Reno, T., et al. (2011). Reversed-phase chromatography with multiple fraction concatenation strategy for proteome profiling of human MCF10A cells. Proteomics *11*, 2019–2026.

61. Paulo, J.A., O'Connell, J.D., Everley, R.A., O'Brien, J., Gygi, M.A., and Gygi, S.P. (2016). Quantitative mass spectrometry-based multiplexing compares the abundance of 5000 S. cerevisiae proteins across 10 carbon sources. J. Proteomics *148*, 85–93.

62. Beausoleil, S.A., Villén, J., Gerber, S.A., Rush, J., and Gygi, S.P. (2006). A probability-based approach for high-throughput protein phosphorylation analysis and site localization. Nat. Biotechnol. *24*, 1285–1292.

63. Elias, J.E., and Gygi, S.P. (2007). Target-decoy search strategy for increased confidence in large-scale protein identifications by mass spectrometry. Nat. Methods *4*, 207–214.

64. Elias, J.E., and Gygi, S.P. (2010). Target-decoy search strategy for mass spectrometry-based proteomics. Methods Mol. Biol. *604*, 55–71.

65. McAlister, G.C., Huttlin, E.L., Haas, W., Ting, L., Jedrychowski, M.P., Rogers, J.C., Kuhn, K., Pike, I., Grothe, R.A., Blethrow, J.D., and Gygi, S.P. (2012). Increasing the multiplexing capacity of TMTs using reporter ion isotopologues with isobaric masses. Anal. Chem. *84*, 7469–7478.

STAR★METHODS

KEY RESOURCES TABLE

REAGENT or RESOURCE	SOURCE	IDENTIFIER
Chemicals, peptides, and recombinant proteins		
Urea	MilliporeSigma	Cat#U5128-500G
Methanol	MilliporeSigma	Cat#MX0486
Chloroform	MilliporeSigma	Cat#C2432
Water	Thermo Fisher Scientific	Cat#W61
Bond-Breaker TCEP	Thermo Fisher Scientific	Cat#77720
Trypsin protease	Thermo Fisher Scientific	Cat#90059
LysC protease	FUJIFILM Wako Pure Chemical Corporation	Cat#12902541
Acetonitrile	VWR BDH chemicals	Cat#BDH83639.100E
C18 Sep-Pak (500 mg)	Waters	Cat#WAT036945
StageTip Empore C18 material	3M	Cat#14-386-2
EPPS	MilliporeSigma	Cat#E9502
TFA	Thermo Fisher Scientific	Cat#102164
Formic acid	Thermo Fisher Scientific	Cat#85178
DTT	Thermo Fisher Scientific	Cat#R0861
Anhydrous acetonitrile	Honeywell Burdick & Jackson	Cat#AS017-0100
50% hydroxylamine	Thermo Fisher Scientific	Cat#90115
Accucore C18 resin, 2.6 μm, 150 Å	Thermo Fisher Scientific	Cat#16126-000
rmEgf	Thermo Fisher Scientific	Cat#2028EG200
PD-0325901	Selleck	Cat#S1036
Hydroxypropyl methylcellulose	VWR	Cat#44779.18
Iodoacetamide	Thermo Fisher Scientific	Cat#A39271
Beta-mercaptoethanol	Thermo Fisher Scientific	Cat#21985-023
cOmplete™ EDTA-free protease nhibitor cocktail	MilliporeSigma	Cat#11873580001
Phosphatase Inhibitor Cocktail 2	MilliporeSigma	Cat#P5726
Phosphatase Inhibitor Cocktail 3	MilliporeSigma	Cat#P0044
Phosphate buffered saline	Thermo Fisher Scientific	Cat#MT21040CV
DMSO	Thermo Fisher Scientific	Cat#D12345
Ammonium bicarbonate	Sigma	Cat#285099
Critical commercial assays		
BCA assay	Thermo Fisher Scientific	Cat#A55864
TMTpro16plex Isobaric Label Set	Thermo Fisher Scientific	Cat#A44520
High-Select Fe-NTA Phosphopeptide Enrichment Kit	Thermo Fisher Scientific	Cat#A32992
RNeasy Plus Mini Kit	Qiagen	Cat#74136
Deposited data		
Proteomics data	This paper	ProteomeXchange Consortium: PXD050402
RNAseq data	This paper	NCBI GEO: GSE262676
Custom code	This paper	https://github.com/Beawasthi/Egf-signaling
Experimental models: Organisms/strains		
Wild-type C57BL/6J	The Jackson laboratory	JAX: 000664

(*Continued on next page*)

Continued

REAGENT or RESOURCE	SOURCE	IDENTIFIER
Software and algorithms		
UpSetR	Conway et al.[47]	https://github.com/hms-dbmi/UpSetR
VennDiagram	Chen & Boutros[48]	https://github.com/uclahs-cds/package-VennDiagram
clusterProfiler	Wu et al.[49]	https://guangchuangyu.github.io/software/clusterProfiler/
DEseq2	Love et al.[50]	https://github.com/thelovelab/DESeq2
MSstats	Kohler, Staniak et al.[51]	https://github.com/Vitek-Lab/MSstats
MSstatsTMT	Huang et al.[52]	https://github.com/Vitek-Lab/MSstatsTMT
MSstatsPTM	Kohler, Tsai et al.[29]	https://github.com/Vitek-Lab/MSstatsPTM
dendextend	Galili[53]	https://github.com/talgalili/dendextend
lme4	Bates et al.[54]	https://github.com/lme4/lme4
lmerTest	Kuznetsova et al.[55]	https://github.com/runehaubo/lmerTestR
ggfortify	Tang et al.[56]	https://github.com/sinhrks/ggfortify
ggsignif	Ahlmann-Eltze & Patil[57]	https://github.com/const-ae/ggsignif
DOSE	Yu et al., 2015[58]	https://github.com/YuLab-SMU/DOSE
Comet-based pipeline	In-house	https://uwpr.github.io/Comet/
MSconvert	Chambers et al.[59]	https://proteowizard.sourceforge.io/download.html
Mouse protein reference database	Uniprot	https://www.uniprot.org (dataset downloaded: August 2021)
Other		
Orbitrap Eclipse mass spectrometer	Thermo Fisher Scientific	Cat#FSN04-10000
Exploris480 mass spectrometer	Thermo Fisher Scientific	Cat#BRE725539
Orbitrap Fusion Lumos mass spectrometer	Thermo Fisher Scientific	Cat#IQLAAEGAAPFADBMBHQ
Agilent 1200 pump	Agilent	Cat#G1361-90011

EXPERIMENTAL MODEL AND STUDY PARTICIPANT DETAILS

Animal models

All experiments were performed using female wild-type C57Bl/6J mice purchased from Jackson laboratory (Stock no. 000664) that were aged 10–12 weeks. Mice were housed in a barrier facility within a temperature-controlled environment and 12-h light/dark cycle and fed *ad libitum*. All experiments were approved by the Institutional Animal Care and Use Committee (IACUC) at Dana-Farber Cancer Institute and followed IACUC guidelines for the ethical care and use of experimental animals.

METHOD DETAILS

Mouse treatments and tissue collection

For phosphoproteomic/proteomic experiments, mice were treated with 1 mg/kg recombinant mouse Egf (rmEgf (Thermo Fisher Scientific #2028EG200), 0.4 mg/mL stock in phosphate buffered saline (PBS) (Thermo Fisher Scientific #MT21040CV)), 10 mg/kg PD-0325901 (Meki) (Selleck #S1036) (90 mg/mL in DMSO (Thermo Fisher Scientific #D12345)/hydroxypropyl methylcellulose (VWR #44779.18)), a combination of the two, or vehicle controls. Vehicle controls for Meki and Egf were administered to mice treated with Egf but not Meki and Meki but not Egf, respectively, to ensure that all treated mice were handled equivalently. Egf was administered by retro-orbital injection 15 min prior to harvest under isoflurane anesthesia. Meki treatments were administered by oral gavage 2 h prior to harvest. Mice were euthanized by cervical dislocation, and organs were rapidly harvested and flash-frozen.

For transcriptomic experiments, 1 mg/kg of rmEgf or PBS was administered by retro-orbital injection under isoflurane anesthesia 2 h and 6 h before euthanasia. Mice were euthanized by cervical dislocation and organs rapidly harvested and flash-frozen. Three untreated control mice were included for both phosphoproteomic/proteomic and transcriptomic experiments.

Sample preparation for phosphoproteomics/proteomics

Mass spectrometry preparation was performed as previously described.[28] Briefly, tissues were pulverized in liquid nitrogen and lysed with a needle/syringe in 8M urea (Millipore Sigma #U5128-500G)/200mM EPPS (MilliporeSigma #E9502) buffer (pH 8.5) with protease

and phosphatase inhibitors (1X – 2X cOmplete EDTA-free protease inhibitor cocktail (MilliporeSigma #11873580001), 1X – 2X Phosphatase Inhibitor Cocktail 2 (MilliporeSigma #P5726), and 1X – 2X Phosphatase Inhibitor Cocktail 3 (MilliporeSigma #P0044)). Lysed tissues were pelleted at 4 °C at 14,000 rpm and the supernatant was isolated for subsequent steps. A Bicinchoninic acid (BCA) assay (Thermo Fisher Scientific #A55864) was used to determine protein concentration according to manufacturer's instructions. Samples were adjusted to 1 mg/mL and 200 μg of protein were reduced with 5mM TCEP (Thermo Fisher Scientific #77720) for 15 min and alkylated with 10mM iodoacetamide (Thermo Fisher Scientific #A39271) for 30 min. Quenching was performed with 5mM dithiothreitol (DTT) (Thermo Fisher Scientific #R0861) for 15 min. The reduced and alkylated protein was precipitated with methanol/chloroform (4 methanol (MilliporeSigma #MX0486): 1 chloroform (MilliporeSigma #C2432): 3 water (Thermo Fisher Scientific #W61)) and reconstituted in 200 μL of 200mM EPPS (MilliporeSigma #E9502) buffer (pH 8.5). Proteins were digested overnight with LysC protease (FUJIFILM Wako Pure Chemical Corporation #12902541) at room temperature (1:50 LysC-to-peptide ratio) and with trypsin protease (Thermo Fisher Scientific #90059) for 6h the next day at 37°C (1:100 trypsin-to-peptide ratio). Following trypsin digest, 30 μL of anhydrous acetonitrile (Honeywell Burdick & Jackson AS017-0100) were added for every 100 μL digest and 200 μg peptide were labeled with 400 μg TMT using TMTpro16plex Isobaric Labels (Thermo Fisher Scientific #A44520). Quenching of the labeling reaction was achieved by addition of 50% hydroxylamine (only for individual tissue plexes) (Thermo Fisher Scientific #90115) to a final concentration of 0.3%. To confirm complete labeling and evaluate mixing ratios, 2 μL of each sample was pooled, desalted, and analyzed by mass spectrometry prior to quenching. This "ratio check" was used to calculate normalization factors and samples were mixed at 1:1 ratios across all TMT channels. The combined samples were desalted with a 500mg Sep-Pak solid phase extraction column (Waters #WAT036945) and dried in a vacuum centrifuge. Phosphopeptides were enriched from the labeled sample using the High-Select Fe-NTA Phosphopeptide Enrichment Kit (Thermo Fisher Scientific #A32992) according to the manufacturer's protocol. For phosphopeptide enrichment, the pH of the resuspended peptides should be less than 3.0. Formic acid was used to adjust sample pH of some samples prior to enrichment to be less than 3.0. For all samples, we prepared an "elution collection tube" with 20 μL of 100% formic acid (Thermo Fisher Scientific #85178), into which the eluates were eluted. The combined eluate was vacuum centrifuged to near dryness and desalted via StageTip. StageTip Empore-C18 material was purchased from 3M, St. Paul, MN (#14-386-2). Fractions were collected in a 96-well plate and combined into 12 fractions that were desalted and analyzed by LC-MS/MS analysis to serve as the total proteome corresponding to each phosphoproteome as described below.

Offline basic pH reversed-phase (BPRP) fractionation for whole proteome TMT-based experiment

We fractionated the pooled, labeled peptide sample using BPRP HPLC[60] and an Agilent 1260 pump equipped with a degasser and a UV detector (set at 220 and 280 nm wavelength). Peptides were subjected to a 50-min linear gradient from 5% to 35% acetonitrile (VWR BDH chemicals #BDH83639.100E) in 10 mM ammonium bicarbonate (Sigma #285099) pH 8 at a flow rate of 0.6 mL/min over an Agilent 300Extend C18 column (3.5 μm particles, 4.6 mm ID and 250 mm in length). The peptide mixture was fractionated into a total of 96 fractions, which were consolidated into 24 super-fractions,[61] all of which were analyzed. Samples were subsequently acidified with 1% formic acid and vacuum centrifuged to near dryness. Each super-fraction was desalted via StageTip, dried again via vacuum centrifugation, and reconstituted in 5% acetonitrile, 5% formic acid for LC-MS/MS processing.

Mass spectrometry data acquisition

For the individual tissue TMT plexes of the phosphoproteome, mass spectrometry data were collected using an Orbitrap Eclipse mass spectrometer (Thermo Fisher Scientific, San Jose, CA) coupled with Vanquish *Neo* liquid chromatograph. Peptides were separated on a 100 μm inner diameter microcapillary column packed with ~30 cm of Accucore C18 resin (2.6 μm, 150 Å, Thermo Fisher Scientific #16126-000). For each analysis, we loaded ~2 μg onto the column. Peptides were separated using a 150 min gradient of 5–29% acetonitrile in 0.125% formic acid with a flow rate of ~300–400 nL/min. The scan sequence began with an Orbitrap MS^1 spectrum with the following parameters: resolution 60K, scan range 350–1350, automatic gain control (AGC) target 100%, maximum injection time auto, and centroid spectrum data type. The duty cycle was set at 1s/CV and MS^2 analysis which consisted of HCD high-energy collision dissociation with the following parameters: resolution 50K, AGC 250 ms, maximum injection time 300%, isolation window 0.5 Th, normalized collision energy (NCE) 36%, and centroid spectrum data type. Dynamic exclusion was set to automatic. The FAIMS compensation voltages (CV) were −40, −60, −80V and −30, −50, −70V (for a total of 2 injections per sample).

For the total proteome individual tissue plexes, the parameters were the same as for the phosphoproteome, with the following exceptions: 90 min gradient for initial peptide separation and the following MS^2 parameters: isolation window 0.6 Th, AGC 86 ms, maximum injection time 200%. Additionally, for the total proteome individual tissue plexes, the FAIMS compensation voltages (CV) were −40, −60, −80V.

For the phosphoproteome multi-tissue plexes, mass spectrometry data were collected using an Exploris480 mass spectrometer (Thermo Fisher Scientific, San Jose, CA) coupled with nLC-1200 liquid chromatograph. Peptides were separated on a 100 μm inner diameter microcapillary column packed with ~30 cm of Accucore C18 resin (2.6 μm, 150 Å, Thermo Fisher Scientific). For each analysis, we loaded ~2 μg onto the column. Peptides were separated using a 150 min gradient of 5–29% acetonitrile in 0.125% formic acid with a flow rate of ~300–400 nL/min. The scan sequence began with an Orbitrap MS^1 spectrum with the following parameters: resolution 60K, scan range 350–1350, automatic gain control (AGC) target 100%, maximum injection time auto, and centroid spectrum data type. The duty cycle was set at 1s/CV and MS^2 analysis which consisted of HCD high-energy collision dissociation with the following parameters: resolution 30K turbo TMT, AGC 150 ms, maximum injection time 300%, isolation window 0.7 Th, normalized

collision energy (NCE) 36%, and centroid spectrum data type. Dynamic exclusion was set to automatic. The FAIMS compensation voltages (CV) were −40, −60, −80V and −30, −50, −70V (for a total of 2 injections per sample).

Mass spectrometry data for the total proteome multi-tissue plexes were collected using Orbitrap Lumos mass spectrometer (Thermo Fisher Scientific, San Jose, CA) coupled with nLC-1200 liquid chromatograph. Peptides were separated on a 100 μm inner diameter microcapillary column packed with ∼30 cm of Accucore C18 resin (2.6 μm, 150 Å, Thermo Fisher Scientific). For each analysis, we loaded ∼2 μg onto the column. Peptides were separated using a 90 min gradient of 5–29% acetonitrile in 0.125% formic acid with a flow rate of ∼300–400 nL/min. The scan sequence began with an Orbitrap MS^1 spectrum with the following parameters: resolution 60K, scan range 350–1350, automatic gain control (AGC) target 100%, maximum injection time auto, and centroid spectrum data type. The duty cycle was set at 1s/CV and MS^2 analysis which consisted of HCD high-energy collision dissociation with the following parameters: resolution 50K, AGC 120 ms, maximum injection time 200%, isolation window 0.7 Th, normalized collision energy (NCE) 36%, and centroid spectrum data type. Dynamic exclusion was set to automatic. The FAIMS compensation voltages (CV) were −30, −50, −70V.

QUANTIFICATION AND STATISTICAL ANALYSIS

Mass spectrometry data analysis

Spectra were converted to mzXML via MSconvert.[59] Database searching included all entries from the mouse UniProt reference Database (downloaded: August 2021). The database was concatenated with one composed of all protein sequences for that database in reversed order. Searches were performed using a 50-ppm precursor ion tolerance for total protein level profiling. The product ion tolerance was set to 0.03 Da. These wide mass tolerance windows were chosen to maximize sensitivity in conjunction with Comet searches and linear discriminant analysis.[20,62] For TMT experiments, TMTpro labels on lysine residues and peptide N-termini +304.207 Da), as well as carbamidomethylation of cysteine residues (+57.021 Da) were set as static modifications, while oxidation of methionine residues (+15.995 Da) was set as a variable modification. In addition, deamidation (+0.984 Da) at glutamine and asparagine residues and phosphorylation (+79.966 Da) at serine, threonine, and tyrosine residues were also set as variable modifications for phosphopeptide enrichment. Peptide-spectrum matches (PSMs) were adjusted to a 1% false discovery rate (FDR).[63,64] PSM filtering was performed using a linear discriminant analysis, as described previously[20] and then assembled further to a final protein-level FDR of 1%.[20] Proteins were quantified by summing reporter ion counts across all matching PSMs, also as described previously.[65] For phosphosite identification, the AScore[62] false-discovery metric was used and only phosphosites with an AScore of >13 (95% confidence) were considered localized. Proteins were quantified by summing reporter ion counts across all matching PSMs, also as described previously.[65] Reporter ion intensities were adjusted to correct for the isotopic impurities of the different TMTpro reagents according to manufacturer specifications. The signal-to-noise (S/N) measurements of peptides assigned to each protein were summed and these values were normalized so that the sum of the signal for all proteins in each channel was equivalent to account for equal protein loading. Finally, each protein abundance measurement was scaled, such that the summed signal-to-noise for that protein across all channels equals 100, thereby generating a relative abundance (RA) measurement. For phosphopeptides, the RA measurement was calculated at the peptide level.

Normalization and filtering of single-tissue TMT plexes

For clustering, heat maps, and kinase enrichment analysis, the data were normalized using a Comet-based in-house software and subsequently scaled as discussed above.

The phosphoproteome was then filtered based on a threshold of coefficient of variation (CV) across vehicle control samples and Egf-stimulated samples. Specifically, phosphopeptides with a CV > 0.6 across vehicle control samples or CV > 0.7 across Egf-treated samples in any tissue were filtered out. CV thresholds were chosen based on the minimum needed for samples to cluster by tissue by hierarchical clustering, using the default method (“complete”) within the “hclust” function in r.

To calculate Egf-stimulated phosphorylation fold-changes and phosphorylation changes following Egf + Meki treatment for each phosphopeptide, TMT values for each replicate of Egf- or Egf + Meki-treated samples were normalized to the mean of the TMT values for all vehicle control samples for that phosphopeptide.

Kinase enrichment analysis

Kinase enrichment analysis[30] was performed using the Enrichment Analysis tool on PhosphoSitePlus.[35] A log fold-change threshold of absolute value 1 and *p*-value threshold of 0.05 were used for the foreground set definition. Significantly enriched kinases were selected as those with an adjusted enrichment *p*-value of less than 0.05.

For Egf-treated samples, kinase enrichment analysis was performed on the fold-change of the mean of the Egf-treated TMT values determined using in-house software compared with the mean of the vehicle-treated TMT values for each tissue. For Egf + Meki -treated samples, kinase enrichment analysis was performed on the fold-change of the mean of the Egf + Meki -treated values compared with the mean of the vehicle-treated values for each tissue.

Significance analysis of phosphorylation changes within single tissue plexes

For all significance analyses for phosphorylation changes within the single tissue plexes, MSstatsPTM[29] on raw intensities was used to calculate a fold-change and FDR-adjusted *p*-value for all Egf - to - vehicle control and Egf + Meki - to - vehicle control comparisons.

The dataSummarizationPTM_TMT function was implemented using the parameters MPimpute.PTM = FALSE and maxQuantileforCensored = 0.999 and the default for all other parameters for post-translational modification (PTM) and protein-level data summarization. Differential analysis was performed using the groupComparisonPTM function with default parameters. PTM levels adjusted for protein levels were used to identify phosphopeptides that were significantly changed in response to Egf stimulation. Significant comparisons were identified as with abs($\log_2$(fold-change)) > $\log_2$(1.5) and the FDR-adjusted p-value <0.05.

Correlation of fold-changes calculated by MSstatsPTM versus in-house software in single-tissue plexes

Pearson correlation was used for correlation analysis of Egf-stimulated fold-changes in phosphopeptide levels calculated using MSstatsPTM and our Comet-based in-house software. For this analysis, the fold-changes plotted from the in-house software were calculated as discussed above and averaged.

Gene ontology analysis for phosphoproteome

Gene ontology analysis on phosphoproteins was performed using the enrichGO function of clusterProfiler.[49] For analysis of ontologies enriched in response to Egf stimulation within each tissue, proteins with at least one significant phosphorylation change in the Egf-treated samples compared with vehicle control based on MSstatsPTM analysis were used as input. To identify Mapk-dependent Egf-regulated ontologies, significantly changed phosphorylation sites between the Egf- and vehicle control-treated samples were first filtered to include only those that were significantly different between the Egf- and Egf + Meki treated group based on MSstatsPTM analysis. Protein with at least one phosphorylation site fitting these criteria were used as input for the gene ontology analysis. For each analysis, proteins detected in either the phosphoproteome or total proteome of a given tissue were included as the background for that tissue. Benjamini-Hochberg correction was performed, and significant ontologies were selected using the following parameters: pvalue cutoff (for both unadjusted and adjusted pvalue) 0.05 and qvalue cutoff 0.05. Dotplots were generated using DOSE.[58]

Normalization of multi-tissue TMT plexes

Initially, each TMT plex was scaled to 100 on both the phosphoproteome and total proteome level as described above. Within each plex, z-scores were calculated for all 8 bridge samples. Pearson correlation coefficients were calculated for the z-scores of all 8 bridge samples for each peptide between the two plexes. For the phosphoproteome, each plex was filtered so that the correlation coefficient between the z-scores of the bridge samples for each phosphopeptide was greater than 0.9. For the total proteome, each plex was filtered so that 1 of 2 criteria were met on the total protein level: 1) there were greater than 3 peptides detected for a given protein or 2) the correlation coefficient between the z-scores of the bridge samples for a protein was greater than 0.9. To merge the two plexes for both the phosphoproteome and total pro teome, the mean of the bridge samples within the non-scaled plexes was calculated for each phosphopeptide in the phosphoproteome and each protein in the total proteome, and each phosphopeptide and protein was divided by the mean of the bridge for that phosphopeptide/protein. The average of each replicate used as a bridge channel was used as the representative value for that replicate in the final merged dataset. Following normalization, each merged TMT plex was subsequently scaled to 100 on the phosphopeptide/protein level.

Shannon entropy analysis

Tissue-specificity of each protein was calculated using Shannon entropy[33] analysis as was previously done.[20] An entropy value using the equation $H(A) = -\sum_t p(A_t) ln(p(A_t))$ (where H represents entropy, t indicates a tissue, and A represents relative abundance) was calculated separately for each protein that passed filtering criteria. Entropy values were calculated within each scaled TMT plex, prior to bridge-normalization. To ensure that zero values did not pose an issue, 1/16 was added to each TMT value for each sample. The threshold for tissue-specificity for proteins was set 2.58. This threshold is equivalent to the entropy value if each sample from two tissues contributed 10% of the signal for a given protein and each sample from the other two tissues contributed 2.5% of the signal (80% of the signal from two tissues and 20% from the other two tissues). A protein was considered tissue-enriched in a tissue if the average entropy value between both TMT plexes was less than 2.58 and at least 25% of the signal for that protein came from the tissue in both plexes.

Linear mixed models

Linear mixed models were fit for phosphorylation levels as a function of total protein level, treatment, tissue type, and the interaction between treatment and tissue type as fixed effects and replicate as a random effect, were generated using the lmerTest package in R according to the following equation:

$$y_{jter} = \mu + total\ abundance_j + tissue_t + treatment_e + (tissue * treatment)_{te} + replicate_r + \varepsilon_{jter}\ replicate_r\ i.i.d. \approx N(0, \sigma^2)$$

Here, the level of a given phosphopeptide of protein j is written as a function of the total abundance of the protein j, within the tissue t in response to a treatment e within each replicate r.

The bridge-normalized, merged, and scaled total proteome and phosphoproteome were used as input to generate the model. Replicate was included as a random effect to account for variation due to sample preparation, TMT channels, and mass spectrometry runs. Treatment, tissue type, and replicate were included as categorical variables that were encoded as dummy variables within the model. The heart vehicle control was used as the reference level.

RNA-seq library preparation

RNA extraction was performed on mouse tissues using the Qiagen RNeasy Plus Mini kit (Qiagen # 74136). Flash-frozen tissues were pulverized in liquid nitrogen and lysed directly in the provided Buffer RLT Plus containing beta-mercaptoethanol (Thermo Fisher Scientific #21985-023) prior to RNA extraction according to the manufacturer's instructions. Subsequent RNA isolation steps were performed according to the manufacturer's instructions. RNA was eluted into RNase-free water.

RNA quality control, library preparation, and sequencing were performed by Novogene according to standard practice. Prior to library preparation, sample QC was performed by Novogene using an Agilent 5400 Bioanalyzer. All samples had RIN >9. Library preparation was performed using polyA enrichment and sequencing was performed via Illumina platforms using a paired-end 150 bp sequencing strategy with 20 million reads per sample.

mRNA quality control and read alignment

Quality control and alignment of mRNA libraries was performed by Novogene. Briefly, raw read data were processed by in-house perl scripts to remove reads containing adapter or poly-N (N > 10%) and low-quality reads (Base Quality <5 comprises more than 50% of the read). Hisat2 v2.0.5 was used as the mapping tool for read alignment using mm39 as the reference genome. Read counts were calculated using featureCounts v1.5.0-p3.

mRNA differential expression analysis

Differential gene expression analysis was performed using DESeq2.[50] To identify differentially expressed genes between Egf- and vehicle control-treated samples in each tissue, normalization and differential gene expression analysis were separately performed using the DEseq function within each tissue. The design formula included a single "group" variable to represent each treatment/time-point group. Prior to normalization, the transcriptomic dataset for each tissue was filtered so that at least 3 samples had a read count per gene greater than 10. Significant DEGs within each tissue were considered as those with Benjamini-Hochberg adjusted FDR <0.05 and absolute value $\log_2$(fold-change) > 1.

Gene ontology analysis for transcriptome

Gene ontology analysis on significant upregulated DEGs within each tissue was performed using the enrichGO function of clusterProfiler.[49] Significant upregulated DEGs within each tissue were identified using DESeq2 as described above, where significant genes were classified as those with Benjamini-Hochberg FDR < 0.05 and abs($\log_2$(fold-change)) > 1. For each analysis within each tissue, all genes detected within the filtered transcriptomic dataset for that tissue (as described above) were used as the background. Benjamini-Hochberg FDR correction was performed, and significant ontologies were selected using the following parameters: pvalue cutoff (for both unadjusted and adjusted pvalue) 0.05 and qvalue cutoff 0.05. Dotplots were generated using DOSE.[58]

Hierarchical clustering analysis

Hierarchical clustering analysis on the phosphoproteome and proteome was performed using the hclust() function in R. For clustering of phosphoproteome fold-changes in response to Egf, 0.01 was added to all fold-changes and (fold-changes +0.01) were log-transformed prior to clustering. Clustering was performed using the "ward.D2" method. Dendrograms were produced using the dendextend package.[53]

Principal component analysis

Principal component analysis (PCA) on the phosphoproteome and proteome was performed using the prcomp() function with centered and scaled data.

PCA on the transcriptome was performed using an adapted version of the plotPCA function from DESeq2 (see code), using gene expression data normalized across all tissues using the DESeq2 function. Prior to normalization, the transcriptomic dataset was filtered so that at least 3 samples had a read count per gene greater than 10. Prior to the PCA, a variance stabilizing transformation was performed on the normalized dataset using the vst function using the parameter "blind = FALSE". For correlation of PCs with tissue type, treatment/time-point, and treatment type, the following variables were used: heart, lung, kidney, or liver for tissue type, Egf (2h), Egf (6h), and no Egf (containing all vehicle and untreated samples irrespective of time-point) for treatment/time-point, and Egf (containing all Egf-treated samples irrespective of time-point) and no Egf (containing all vehicle and untreated samples irrespective of time-point) for treatment type.

Volcano plots

Volcano plots were generated using ggplot2 in R. For volcano plots of phosphoproteomic fold-changes, FDR-adjusted *p*-values and $\log_2$(fold-changes) were calculated using MSstatsPTM.[29] For volcano plots of transcriptomic changes, FDR-adjusted *p*-values and $\log_2$(fold-changes) were calculated using the DEseq2 package.[50]

UpSet plots

UpSet plots were generated using the UpSetR package[47] in R to analyze common proteins, phosphoproteins, phosphopeptides, genes, and their respective changes in response to treatment as described in the text.